Manuscript prepared for Atmos. Chem. Phys.
with version 2014/09/16 7.15 Copernicus papers of the LATEX class copernicus.cls.
Date: 30 August 2018

Changes in the aerosol direct radiative forcing from 2001 to 2015: observational constraints and regional mechanisms

Fabien Paulot[1,2], David Paynter[1], Paul Ginoux[1], Vaishali Naik[1], and Larry W. Horowitz[1]

[1]Geophysical Fluid Dynamics Laboratory, National Oceanic and Atmospheric Administration, Princeton, New Jersey, USA
[2]Program in Atmospheric and Oceanic Sciences, Princeton University, New Jersey, USA

Correspondence to: Fabien.Paulot@noaa.gov

Abstract. We present estimates of changes in the direct aerosol effects (DRE) and its anthropogenic component (DRF) from 2001 to 2015 using the GFDL chemistry-climate model AM3 driven by CMIP6 historical emissions. AM3 is evaluated against observed changes in the clear-sky short-wave direct aerosol effect (DRE_{sw}^{clr}) derived from the Clouds and the Earth's Radiant Energy System

5 (CERES) over polluted regions. From 2001 to 2015, observations suggest that DRE_{clr}^{sw} increases (i.e., less radiation is scattered to space by aerosols) over Western Europe ($0.7 - 1\ \mathrm{W\,m^{-2}\,decade^{-1}}$) and the Eastern US ($0.9 - 1.8\ \mathrm{W\,m^{-2}\,decade^{-1}}$), decreases over India ($-0.5 - -1.9\ \mathrm{W\,m^{-2}\,decade^{-1}}$), and does not change significantly over Eastern China. AM3 captures these observed regional changes in DRE_{clr}^{sw} well in the US and Western Europe, where they are dominated by the decline of sulfate

10 aerosols, but not in Asia, where the model overestimates the decrease of DRE_{clr}^{sw}. Over India, the model bias can be partly attributed to a decrease of dust optical depth, which is not captured by our model and offsets some of the increase of anthropogenic aerosols. Over China, we find that the decline of SO_2 emissions after 2007 is not represented in the CMIP6 emission inventory. Accounting for this decline using the Modular Emission Inventory for China and for the heterogeneous oxidation

15 of SO_2 significantly reduce the model bias. For both India and China, our simulations indicate that nitrate and black carbon contribute more to changes in DRE_{clr}^{sw} than in the US and Europe. Indeed, our model suggests that black carbon ($+0.12\ \mathrm{W\,m^{-2}}$) dominates the relatively weak change in DRF from 2001 to 2015 ($+0.03\ \mathrm{W\,m^{-2}}$). Over this period, the change in the forcing from nitrate and sulfate are both small and of the same magnitude ($-0.03\ \mathrm{W\,m^{-2}}$ each). This is in sharp contrast to

20 the forcing from 1850 to 2001 in which forcings by sulfate and black carbon largely cancel each others, with minor contributions from nitrate. The differences between these time periods can be

well understood from changes in emissions alone for black carbon but not for nitrate and sulfate, which reflects non-linear changes in their photochemical production associated with changes in both the magnitude and spatial distribution of anthropogenic emissions.

25 **1 Introduction**

Aerosols affect climate (Boucher et al., 2013) both directly, via scattering and absorption of solar and terrestrial radiation (Charlson et al., 1992), and indirectly, by modulating the abundance of cloud condensation nuclei, the droplet size distribution, and the lifetime of clouds (Twomey, 1974; Rosenfeld et al., 2014). Storelvmo et al. (2016) estimated that the increase in the burden of atmospheric
30 aerosols associated with anthropogenic activities has masked approximately one-third of the continental warming from greenhouse gases from 1964 to 2010, with important implications for global and regional climate (Wild, 2009; Bollasina et al., 2011).

Previous studies have leveraged global spaceborne observations of the Earth's radiative budget (Wielicki et al., 1996, 1998) and aerosol abundance (Kahn et al., 2005; Levy et al., 2013b) to es-
35 timate the overall aerosol direct radiative effect (DRE), i.e., the direct perturbation of the Earth's radiative budget by aerosols (Christopher and Zhang, 2004; Patadia et al., 2008; Loeb and Manalo-Smith, 2005; Kahn, 2012). Observational constraints for the aerosol direct radiative forcing (DRF), the anthropogenic component of the aerosol direct radiative effect, are less robust (Su et al., 2013; Bellouin et al., 2005, 2008), which contributes to the large spread in model estimates for DRF in
40 2000 relative to 1850 (-0.02 – -0.58 $\mathrm{W\,m^{-2}}$ Myhre et al. (2013)). In particular, the sensitivity of the aerosol direct radiative forcing to anthropogenic emissions remains uncertain. Previous work has shown that the aerosol forcing simulated by global climate models from 1850 to 2001 is well correlated with changes in SO_2 emissions (Stevens, 2015). However, this relationship may not be applicable in recent years and for future conditions, as the spatial distribution and speciation of
45 anthropogenic emissions evolve (Stevens et al., 2017).

In this work, we aim to provide observational constraints on the sensitivity of the direct aerosol forcing to anthropogenic emissions. The paper is organized as follows: First, we derive an estimate of changes in the clear-sky shortwave aerosol direct radiative effect from 2001 to 2015 constrained by the observed variability in outgoing shortwave radiation from the Clouds and the Earth's Radiant
50 Energy System (CERES). Second, we focus on large source regions of anthropogenic emissions (US, Europe, India, and Eastern China), where observed changes in the aerosol effect are expected to be dominated by anthropogenic aerosols. This allows us to assess whether a state-of-the-art chemistry-climate model (Geophysical Fluid Dynamics Laboratory (GFDL) AM3) driven by the latest emissions from the Coupled Model Intercomparison Project phase 6 can capture changes in the direct
55 radiative forcing from aerosols over the 2001–2015 period. Finally we use AM3 to compare the

sensitivity of the aerosol direct radiative forcing to anthropogenic emissions from 1850 to 2001 and from 2001 to 2015.

2 Methods

2.1 GFDL-AM3 model

60 We use the GFDL-AM3 model (Donner et al., 2011; Naik et al., 2013), the atmospheric chemistry climate component of the GFDL-CM3 model (Donner et al., 2011; Griffies et al., 2011; John et al., 2012). The model is run from 2000 to 2015, using the first year to spin up the model. The model horizontal resolution is $\simeq 200$ km with 48 vertical levels. To facilitate comparisons with synoptic observations, the model horizontal winds are nudged to 6-hourly horizontal winds from the National

65 Centers for Environmental Predication reanalysis (Kalnay et al., 1996). Monthly sea surface temperature and sea ice concentration are prescribed following Taylor et al. (2000) and Rayner et al. (2003), respectively. The configuration of AM3 used in this study includes revisions to the representation of the wet scavenging of chemical tracers by snow and convective precipitation and to the treatment of sulfate and nitrate chemistry, which significantly improve the representation of aerosols. We refer the

70 reader to our recent work for a detailed evaluation of the aerosol simulation in AM3 (Paulot et al., 2016).

The radiative transfer scheme takes into account the aerosol optical properties of sulfate, sea salt, dust, black carbon, organic carbon (Donner et al., 2011) and nitrate (Paulot et al., 2017b). Aerosols are assumed to be externally mixed, except for hydrophilic black carbon and sulfate (Donner et al.,

75 2011). Hygroscopic growth is capped at 95% for all aerosols.

We use the historical anthropogenic emissions developed by the Community Emission Data System (CEDS v2017-05-18) in support of CMIP6 (Hoesly et al., 2018). As anthropogenic emissions are available until 2014 from CEDS, we repeat CEDS 2014 anthropogenic emissions for 2015. Monthly biomass burning emissions are from the historical global biomass burning emissions inventory for

80 CMIP6 (BB4CMIP6, van Marle et al. (2017)). Emissions for the 1997 to 2015 period in this inventory have been derived from satellite-based emissions from the Global Fire Emissions Database (GFED, van der Werf et al. (2017)). The vertical distribution of biomass burning emissions is taken from Dentener et al. (2006). Natural emissions are based on Naik et al. (2013), except for isoprene emissions, which are calculated interactively using the Model of Emissions of Gases and Aerosols

85 from Nature (MEGAN, Guenther et al. (2006)).

Fig. 1 shows changes in the anthropogenic emissions of sulfur dioxide (SO_2), ammonia (NH_3), black carbon (BC), and nitrogen oxide (NO) from 2001 to 2015. Globally, anthropogenic emissions of NH_3, BC, and NO have increased by 18%, 36%, and 16% over the 2001-2015 period, respectively, while SO_2 emissions have remained nearly stable, peaking in 2006. In the US and Europe, there have

90 been significant declines in SO_2 (-71% and -66%, respectively) and NO (-48% and -39%) emissions,

while NH_3 and BC emissions have changed little (<15%). Indian emissions of SO_2, NO, and BC have increased by 89%, 39%, and 89%. Similarly, Chinese emissions of SO_2, NO, and BC have increased by 56%, 69%, and 93%, respectively. Anthropogenic emissions in India and China are expected to be more uncertain than in the US and Europe (Saikawa et al., 2017a, b). For instance, Fig. 1 shows differences between emissions from CMIP6 and emissions from the regional Modular Emission Inventory for China (MEIC) (Zhang et al., 2009). Unlike in CMIP6, emissions of SO_2 decline starting in 2006, a decrease that accelerates in 2012, while NO emissions decrease after 2012 and BC emissions remain near-stable after 2007. In 2014, MEIC NO, SO_2, and BC emissions are 24%, 48%, and 32% lower than CMIP6 emissions, respectively. NH_3 emissions are similar in magnitude but exhibit different seasonality: CMIP6 NH_3 emissions peak in spring, while MEIC exhibits a broad peak in summer, consistent with top-down constraints (Paulot et al., 2014; Zhang et al., 2017). The impact of these emission uncertainties on the simulated change in the aerosol effect over India and China will be discussed in sections 3.2.2 and 3.2.3, respectively.

2.2 Aerosol direct effect and forcing

The instantaneous aerosol direct radiative effect (DRE) is defined as the difference between the outgoing radiation at the top of the atmosphere (TOA) in the absence and in the presence of aerosols (Heald et al., 2014). The direct radiative forcing (DRF) is defined as the anthropogenic component of the direct radiative effect. In our notation we use the superscript sw to denote the shortwave component of DRE or DRF. Likewise, the subscript clr denotes the clear-sky component of DRE or DRF.

To better isolate the effect of aerosol variability on radiative fluxes, we will focus on the aerosol shortwave direct radiative effect under clear-sky conditions (DRE_{clr}^{sw}):

$$DRE_{clr}^{sw} = rsutcsaf - rsutcs \tag{1}$$

where we use the CMIP6 convention (CMIP6 Data Request, 2018) to designate the outgoing clear-sky shortwave radiation with (rsutcs: radiation shortwave up toa clear sky) and without aerosols (rsutcsaf: radiation shortwave up toa clear sky aerosol free), respectively. For simplicity, we will refer to the aerosol shortwave direct radiative effect under clear-sky conditions (DRE_{clr}^{sw}) as the aerosol effect, hereafter. Note that an increase of the aerosol direct effect indicates a decrease of the radiation scattered to space by aerosols.

2.2.1 Model

In AM3, the aerosol effect is estimated by calling the radiative transfer scheme twice, with and without aerosols (Paulot et al., 2017b) in the absence of clouds. The effect of individual aerosol components is estimated as the difference in outgoing shortwave radiation with and without aerosol x, where x can be sulfate, nitrate, black carbon, organic carbon, dust, sea salt, and stratospheric

125 volcanic aerosols. In the following, we will focus primarily on changes in sulfate and nitrate, which dominate changes in aerosol scattering, and black carbon, which dominates changes in aerosol absorption over the 2001–2015 period.

2.2.2 Observations

The Clouds and the Earth's Radiant Energy System (CERES, Wielicki et al. (1996, 1998)) provides
130 constraints on the Earth's radiative budget since 2000. Here, we use the Energy Balanced and Filled product (EBAF, edition 4, Loeb et al. (2018)) to estimate the variability of the clear-sky shortwave outgoing radiation. This product achieves global coverage by combining CERES broadband cloud-free fluxes with MODIS (Moderate Resolution Imaging Spectroradiometer) radiances for regions that are not completely cloud-free at the CERES footprint scale (Loeb et al., 2018).

135 The simplest way in which CERES EBAF data can be used to estimate changes in the aerosol effect is to assume that all variability in the shortwave clear-sky outgoing radiation is the result of changes in aerosols (Stevens and Schwartz, 2012; Xing et al., 2015; Alfaro-Contreras et al., 2017). We will refer to this estimate as $EBAF_R$ hereafter, where R stands for raw. However, other radiative components may contribute to the variability in the outgoing radiation (Stevens and Schwartz,
140 2012). Therefore, a more accurate estimate of the aerosol effect requires removal of the impact of these components from the measured changes in the outgoing radiation. To achieve this, we calculate radiative kernels (e.g., Soden et al. (2008); Shell et al. (2008)) to estimate the variability of the outgoing clear-sky shortwave radiation associated with changes in surface albedo, ozone, and water vapor (see supporting materials and Fig. S1). For water vapor and ozone, we use the Goddard Modeling
145 and Assimilation Office reanalysis (GEOS5). Since our estimate for the aerosol effect is most sensitive to changes in the surface albedo, we will consider both the albedo from MODIS (Schaaf et al., 2002) and CERES-EBAF (Rutan et al., 2009, 2015; Loeb et al., 2018). Both albedo estimates have been validated extensively and generally show good agreement with observations (Cescatti et al., 2012; Wang et al., 2014b; Rutan et al., 2009, 2015). Estimates of the aerosol effect derived using the
150 MODIS and CERES-EBAF albedo will be referred to as $EBAF_M$ and $EBAF_C$, respectively.

We also derive the change in the aerosol effect from the CERES Synoptic Radiative Fluxes product (SYN, edition 4a). Similar to AM3, the CERES SYN product provides estimates of the radiative fluxes at the top of the atmosphere with and without aerosols present. In the SYN product, the radiative transfer calculations use aerosol properties from the Model for Atmospheric Transport and
155 Chemistry (MATCH), which is constrained by observations from MODIS collection 5 (Collins et al., 2001). Therefore, the SYN calculated aerosol effect is very sensitive to MODIS collection 5 aerosol properties. This collection has now been superseded by MODIS collection 6 (Levy et al., 2013b) and we will discuss some of the implications of differences between MODIS collections 5 and 6 for the derivation of the SYN aerosol effect in sections 3.2.1 and 3.2.2.

2.3 Trend: estimation and interpretation

We use the non-parametric Mann-Kendall test (Kendall, 1938) to identify significant changes in the aerosol effect. This test quantifies monotonic correlations between two variables. It is based on a rank procedure that makes it less susceptible to outliers than the Pearson correlation and thus especially well-suited for the analysis of an environmental dataset. We estimate the linear trend using the Theil-Sen method (Theil, 1950; Sen, 1968). We use a critical p value of 0.05 for trend significance.

Differences between observed and simulated trends in DRE_{clr}^{sw} may reflect biases in the simulated change of the aerosol burden. Here this is diagnosed by comparing the simulated trend in aerosol optical depth (AOD) with those retrieved by the Multi-angle Imaging SpectroRadiometer (MISR) at 555nm (Kahn et al., 2005, 2010) and the MODIS instruments on board the AQUA and TERRA satellites at 550 nm (collection 6, level3, merged deep blue/dark target) (Levy et al., 2013a; Sayer et al., 2014). Note that the accuracy of individual retrievals has been estimated to be $\pm 0.05 \pm 0.15 \times$ AOD (Levy et al., 2010) for MODIS and the maximum of ± 0.05 or $0.2 \times$ AOD for MISR (Kahn et al., 2010).

The change in AOD is not a perfect predictor of changes in DRE_{sw}^{clr} and we will show that it is possible to find regions where observed changes in AOD are well captured by AM3 but not changes in DRE_{sw}^{clr} (see 3.2.2). Such discrepancies may reflect differences in aerosol radiative properties. Specifically, changes in absorbing aerosols, such as black carbon, have a small imprint on AOD but a large one on DRE_{clr}^{sw} (see section 3.2.2 and 3.2.3). Differences in surface properties may also cause differences in DRE_{clr}^{sw} trends. For instance, a lower surface albedo reduces the impact of changes in scattering aerosols on DRE_{sw}^{clr} and conversely increases that of absorbing aerosols. We will show that such differences in surface albedo are important in India (section 3.2.2). However, in other regions, we find they have a small impact on the simulated trend in DRE_{sw}^{clr}.

3 Results

In this section, we will refer to the clear-sky shortwave outgoing radiation (rsutcs) and the aerosol shortwave direct radiative effect under clear-sky conditions (DRE_{clr}^{sw}) as outgoing radiation and aerosol effect, respectively.

3.1 Global distribution of changes in aerosol effect

Fig. 2 shows the decadal rate of change in the aerosol effect, estimated solely from changes in the outgoing radiation ($EBAF_R$) measured by CERES EBAF (top panel) over the 2001–2015 period. We find significant changes (highlighted with dots) in the outflow of the Eastern US, where the radiation scattered back to space by aerosols decreases, and in the outflow of India, where it increases, consistent with the changes in anthropogenic emissions shown in Fig. 1. However, changes

in the outgoing radiation are less significant over the source regions themselves, which highlights the importance of other factors of variability in the outgoing radiation (Stevens and Schwartz, 2012).

195   Fig. 2 also shows the decadal rate of change in the aerosol effect derived from the SYN calculation and from CERES-EBAF outgoing radiation after correction for water, ozone, and surface albedo from MODIS ($EBAF_M$) and CERES-EBAF ($EBAF_C$). All these estimates show better spatial consistency between land and ocean near large sources of anthropogenic pollution than the outgoing radiation alone ($EBAF_R$). In particular, we find that the aerosol effect increases over North America and Europe, and decreases over India. In contrast, the variability is considerably reduced over

200 Australia, Central Asia, and South America, which suggests that it is not primarily associated with aerosols. Consistent with observations, AM3 also shows that the aerosol effect increases over the US and Europe and decreases over India. However, it simulates a decrease in the aerosol effect over China and in the Western Pacific, which is inconsistent with observational constraints.

205   To understand these changes further, we examine the timeseries of the different estimates of the aerosol effect over these regions. $EBAF_R$ exhibits considerable interannual variability over the Eastern US and Europe, with no significant trend (Table S1). In contrast, SYN, $EBAF_C$, and $EBAF_M$ estimates exhibit a significant increase ranging from 0.9 to 1.8 $\mathrm{W\,m^{-2}\,decade^{-1}}$ in the Eastern US and from 0.7 to 1.4 $\mathrm{W\,m^{-2}\,decade^{-1}}$ in Western Europe. AM3 also simulates an increase of the

210 aerosol effect over these regions (0.8 and 0.6 $\mathrm{W\,m^{-2}\,decade^{-1}}$, respectively). The magnitude of these changes is in excellent agreement with $EBAF_M$ but lower than SYN. We refer the reader to section 3.2.1 for a detailed discussion of these regions.

    Over India, most observational estimates (SYN, $EBAF_C$, $EBAF_M$) suggest a decrease of the aerosol effect ($-1.0 - -1.9 \mathrm{W\,m^{-2}\,decade^{-1}}$), which is qualitatively captured by AM3 (-2.4 $\mathrm{W\,m^{-2}\,decade^{-1}}$).

215 However, changes in the outgoing radiation alone ($EBAF_R$) would imply a small increase of the aerosol effect from 2001 to 2015 (0.5 $\mathrm{W\,m^{-2}\,decade^{-1}}$), which suggests that large changes in other radiative components may be masking the aerosol effect. Changes in the aerosol effect over India will be discussed in section 3.2.2.

    Over Eastern China, all observational estimates of the aerosol effect exhibit a rapid decrease from

220 2001 to 2007, followed by an increase until 2015, with no significant trend overall in SYN, $EBAF_C$, and $EBAF_M$. The timing of the reversal is consistent with previous analysis of changes in AOD (Zhao et al., 2017) and outgoing radiation over the China sea (Alfaro-Contreras et al., 2017). AM3 fails to capture this reversal and simulates a significant decrease in the aerosol effect from 2001 to 2015 (-1.3 $\mathrm{W\,m^{-2}\,decade^{-1}}$). Changes in the aerosol effect over China will be discussed in section

225 3.2.3.

    We note that all observation-based estimates of DRE show some significant changes over remote oceanic regions. These changes may reflect cloud contaminations in the CERES cloud filtering algorithm (for $EBAF_C$, $EBAF_M$) and in the aerosol retrieval (SYN). In addition, low aerosol loadings make $EBAF_C$ and $EBAF_M$ more susceptible to errors in the radiative kernels.

 3.2 Regional changes

3.2.1 Western Europe and Eastern US

Fig. 4 (top row) shows the seasonal change of the AOD and aerosol effect over Europe. Observations show that the AOD decreases most in spring and summer (-0.4 dec^{-1} for MODIS TERRA (solid black line), Table 1). This decrease is accompanied by an increase of the aerosol effect of 1–1.8 $W m^{-2} decade^{-1}$ in spring and 1.2–2.5 $W m^{-2} decade^{-1}$ in summer (Fig. 4 (bottom row) and Table 1). AM3 captures these changes well (Table S2). In the model, both changes in AOD and aerosol effect are driven almost entirely by the decrease of sulfate aerosols associated with the decrease of SO_2 emissions. The slower changes in winter and fall reflects the smaller contribution of sulfate to the aerosol burden and the less efficient oxidation of SO_2 in these seasons, which makes sulfate less sensitive to changes in SO_2 emissions (Wang et al., 2011; Paulot et al., 2017a).

Fig. 5 shows the changes of the AOD and aerosol effect over the Eastern US. The overall pattern is similar to Western Europe with large reductions in AOD (up to -0.11 dec^{-1}) and increases in the aerosol effect (up to 3.6 $W m^{-2} decade^{-1}$) in spring and summer (Table 1). AM3 underestimates MODIS AOD as well as the rate of change of the AOD and aerosol effect in summer (Table 1). This is consistent with the model low bias against sulfate concentration in rain water in the US (Paulot et al., 2016). Similar to observations, AM3 also shows greater seasonal contrast between spring and summer in the US than in Europe. In the model, this is driven by more efficient springtime oxidation of SO_2 in Europe, where high emissions of ammonia facilitate its in-cloud oxidation by ozone (Paulot et al., 2017a).

In both Europe and the US, we find that the change in the aerosol effect inferred from the SYN calculation is larger than that estimated from CERES-EBAF outgoing radiation corrected for surface albedo changes ($EBAF_C$ and $EBAF_M$). The magnitude of the changes in the MATCH AOD, which is based on MODIS collection 5 and used to calculated the SYN aerosol effect, is also greater than that inferred from the improved MODIS collection 6 (Table 1). This suggests that the rate of change in SYN aerosol effect may be biased high in Europe and Western Europe.

3.2.2 India

Fig. 6 shows the changes in AOD and aerosol effect over India. We will focus here on changes during the winter (DJF) and premonsoon seasons (MAM).

Previous studies have shown that aerosols are primarily of anthropogenic origin in winter (Babu et al., 2013; Pan et al., 2015). During this season, all instruments show a significant increase in AOD (up to 0.13 dec^{-1}). In spite of this increase, the outgoing radiation ($EBAF_R$) does not exhibit a significant trend. We attribute this apparent inconsistency to a concurrent decrease in surface albedo (Table S3), which may be associated with the increase in the regional greenness leaf area index reported by Zhu et al. (2016). Accounting for changes in surface albedo, we diagnose a decrease

265 in the aerosol effect ranging from -0.8 $W\,m^{-2}\,decade^{-1}$ (using MODIS albedo, $EBAF_M$) to -2.3 $W\,m^{-2}\,decade^{-1}$ (using CERES-EBAF albedo, $EBAF_C$). The large difference between $EBAF_C$ and $EBAF_M$ reflects the difference between MODIS and CERES-EBAF albedo in this region (Table S3).

Fig. 6 shows that the simulated AOD agrees well for both magnitude and trend with MODIS
270 AOD but overestimates the change in MISR AOD (see Table 1). The simulated change in the aerosol effect (-2.7 $W\,m^{-2}\,decade^{-1}$) agrees well with the $EBAF_C$ and SYN estimates (-2.3 and -2.6 $W\,m^{-2}\,decade^{-1}$, respectively). However, this good agreement is fortuitous, as the higher surface albedo in AM3 (0.166) relative to SYN (0.129) or CERES-EBAF (0.135) tends to dampen changes in the simulated aerosol scattering. Specifically, we estimate that the simulated trend in the aerosol
275 effect would be -3.5 $W\,m^{-2}\,decade^{-1}$ if AM3 was forced with the SYN albedo. This suggests that AM3 overestimates the decrease in the aerosol effect by 1 to 2 $W\,m^{-2}\,decade^{-1}$. Many factors could contribute to this bias. Here we focus on the seasonality of the emissions of black carbon and ammonium nitrate precursors. Black carbon is the largest contributor to aerosol absorption over India (+3.2 $W\,m^{-2}$ on average in winter). Its increase cancels out one third (0.9 $W\,m^{-2}\,decade^{-1}$)
280 of the decrease in the aerosol effect, much more than in the US and Europe. This is likely to be an underestimate as the prevalent use of biofuel in winter for heating, a large source of black carbon (Yevich and Logan, 2003; Pan et al., 2015), is not represented in the CMIP6 emission inventory. Nitrate dominates changes in the aerosol scattering in winter (-2.4 $W\,m^{-2}\,decade^{-1}$). This is consistent with previous multi-model assessments, which showed that models that did not include nitrate
285 severely underestimated the AOD over India (Pan et al., 2015). Nitrate is formed via the reaction of ammonia (primarily from agriculture) and nitric acid (from the oxidation of NO, whose emissions are dominated by fossil fuel combustion). Nitrate remains challenging to represent in models because of uncertainties in both ammonia emissions and its chemistry and removal (Heald et al., 2012; Paulot et al., 2016). In particular, the seasonality of Indian ammonia emissions in CMIP6 is based
290 on European emissions and peak in spring. In contrast, Warner et al. (2017) recently showed that the ammonia column peaks in summer over India (Fig. S2). Using AM3, we estimate that modulating ammonia emissions with the seasonality derived from satellite would reduce the simulated trend in the aerosol effect in winter from -2.7 to -1.9 $W\,m^{-2}\,decade^{-1}$. These suggest that uncertainties in the seasonalities of black-carbon and ammonia emissions alone could explain most of the
295 discrepancy between observed and simulated changes in the wintertime aerosol effect.

In the premonsoon season, the AOD changes much less rapidly than in winter (Fig. 6, Table 1). For instance, MODIS (TERRA) AOD increases by 0.04 $decade^{-1}$, less than a third of the rate in winter. This seasonal contrast is not captured by AM3, which simulates a similar change (0.15 $decade^{-1}$) in both seasons (Table 1). This discrepancy can be partly explained by the decrease of dust optical depth
300 (dash black line, -0.07 $decade^{-1}$) diagnosed from MODIS following Ginoux et al. (2012). This decline, which is not captured by AM3, is supported by the decline of coarse-mode aerosols in the

Indo-Gangetic Plain (Babu et al., 2013). Using the simulated relationship between dust optical depth and dust aerosol effect, we estimate that the reduction in dust optical depth has caused an increase in the aerosol effect of 1.4 $\mathrm{W\,m^{-2}\,decade^{-1}}$. This suggests that the decline of dust accounts for most

305   of the discrepancy between the model (-3.1 $\mathrm{W\,m^{-2}\,decade^{-1}}$) and the observational estimates of changes in the aerosol effect (-0.9 – -1.4 $\mathrm{W\,m^{-2}\,decade^{-1}}$).

Jin and Wang (2018) recently suggested that an increase in rainfall in Northwestern India has caused a regional greening, which has been accompanied by a reduction of dust emissions. This mechanism may explain why the Goddard Chemistry Aerosol Radiation and Transport (GOCART),

310   which includes the modulation of dust emissions by LAI (Kim et al., 2013), captures the decrease of dust in this region (Babu et al., 2013). This suggests that the impact of increasing anthropogenic aerosols on the outgoing radiation may have been masked by regional greening both directly (via the decrease of the surface albedo) and indirectly (via lower dust emissions).

3.2.3   Eastern China

315   Fig. 7 shows the change in AOD and aerosol effect over Eastern China. AM3 captures the average magnitude of AOD well in winter and spring but underestimates AOD (MODIS) during the monsoon and post monsoon seasons (Table 1). Although there are significant differences between the different AOD retrievals (Zhao et al., 2017), no significant trend is detected in either AOD or aerosol effect over the entire 2001-2015 period in any season.

320   In contrast to observations, simulated AOD and aerosol effect exhibit significant changes in both spring (0.15 $\mathrm{decade^{-1}}$ and -2.1 $\mathrm{W\,m^{-2}\,decade^{-1}}$, respectively) and summer (0.11 $\mathrm{decade^{-1}}$ and -1 $\mathrm{W\,m^{-2}\,decade^{-1}}$, respectively). In spring, sulfate is the largest contributor to the AOD and aerosol effect but changes are dominated by nitrate aerosols (0.08 $\mathrm{decade^{-1}}$ and -2.2 $\mathrm{W\,m^{-2}\,decade^{-1}}$, respectively (Table 1). This large springtime change in nitrate is associated with the May maximum

325   of ammonia emissions in the CMIP6 emission inventory.

Similar to India, the model bias may be associated with uncertainties in anthropogenic emissions. As noted in section 2.1, there are significant differences between the CMIP6 and MEIC emission inventories for SO_2 after 2007 and NO after 2013 (Fig. 1). A detailed evaluation of these two emission inventories is beyond the scope of this study. However, observations show significant declines

330   in SO_2 columns starting in 2008 (Li et al., 2010; Irie et al., 2016; de Foy et al., 2016; Liu et al., 2016; Ding et al., 2017; van der A et al., 2017; Krotkov et al., 2016) and NO_2 starting in 2012 (Liu et al., 2016; van der A et al., 2017), consistent with MEIC emissions. We refer the reader to the study of van der A et al. (2017) for a detailed discussion of the technological and regulatory changes that have contributed to the changes in Chinese emissions over the 2001-2015 period.

335   To quantify the sensitivity of our results to these uncertainties, we perform another simulation replacing the CMIP6 emission by the MEIC emissions for NO, BC, SO_2, and NH_3 over China. We find that the reduction of SO_2 emissions after 2007 reduces the simulated trend in springtime AOD

by 40% from 0.15 decade^{-1} to 0.09 decade^{-1} in better agreement with observations (Fig. S3). In contrast, the simulated trend of the springtime aerosol effect changes by less than 15% relative to the simulation driven by CMIP6 emissions. This primarily reflects the decrease of both black carbon and SO$_2$ emissions starting in 2007 (Fig. 1), which results in opposite changes in the aerosol effect. Similar to India (in winter), the discrepancy between the model performances for AOD and DRE$_{\text{sw}}^{\text{clr}}$ trends points to a bias in aerosol properties. In particular, MEIC suggests that BC emissions have remained stable from 2005 up to 2013. If instead BC emissions increased over this time period as in the historical CMIP6 emissions, the change in the simulated DRE$_{\text{clr}}^{\text{sw}}$ would be reduced without significant impact on the simulated AOD.

Errors in the representation of the photochemical production of aerosols may also contribute to the model bias. Recent studies have shown that the heterogeneous oxidation of SO$_2$ by NO$_2$ (Cheng et al., 2016) and O$_2$ (Hung and Hoffmann, 2015) at the surface of or in aerosols may be an important source of sulfate in the North China Plains (Wang et al., 2014a; Zheng et al., 2015; Guo et al., 2017; He et al., 2017). To examine the sensitivity of our simulation to this chemistry, we perform an additional simulation using MEIC emissions and the parameterization of the heterogeneous production of sulfate on aerosols from Zheng et al. (2015) (Fig. 8). We find that the heterogeneous oxidation of sulfate increases the simulated sulfate optical depth by 100% in winter and 62% in fall, relative to the simulation driven by MEIC emissions. In contrast, changes are much smaller ($< 25\%$) in spring and summer, which reflects the greater availability of oxidants. The increased production of sulfate in winter and fall results in a stronger link between SO$_2$ emissions and the simulated AOD and aerosol effect (Fig. 8). This stronger link allows the model to better capture some prominent features in the observational record, such as the dip in the aerosol effect in fall 2006 (peak in AOD) or the AOD decrease after 2013. This suggests that both changes to the CMIP6 emissions and to the representation of SO$_2$ photochemistry are needed for AM3 to capture observed changes in the aerosol effect over China from 2001 to 2015.

4 Implication for the aerosol direct forcing

In section 3.2, we have shown that regional differences in the speciation of anthropogenic emissions (e.g., the ratio of ammonia and BC to SO$_2$) and the oxidative environment are important to understand changes in the direct shortwave aerosol radiative effect under clear-sky over the largest sources of anthropogenic pollution.

Fig. 9 shows that the changes in the meridional distribution of BC, NO, NH$_3$ and SO$_2$ anthropogenic emissions between 1850 and 2001 (panel a) and between 2001 and 2015 (panel b). In particular, the 2001–2015 period is characterized by higher emissions of BC (25%), NO (15%), and NH$_3$ (19%) and lower SO$_2$ emissions (-12.5%), relative to the 1850–2001 period. While BC and NH$_3$ emissions have increased in most regions, the change in SO$_2$ and NO emissions is associated

with a decline in the northern midlatitudes and an increase in the tropics. Here, we quantify the associated changes in the meridional distribution of the aerosol direct radiative forcing (DRF), the anthropogenic component of the aerosol direct radiative effect.

The aerosol direct radiative forcing for year y is calculated as:

$$DRF(y) = DRE(anthro = y, met = y) - DRE(anthro = 1850, met = y) \qquad (2)$$

where $anthro$ and met denote the year used for anthropogenic emissions and to nudge the horizontal wind, respectively. Note that we use the same meteorology for both simulations, in order to minimize differences in natural sources (e.g., dust, sea salt, dimethylsulfide). On the basis of our evaluation of AM3, we include MEIC emissions for China, the seasonality of NH_3 from AIRS in India, and the heterogeneous oxidation of SO_2 on aerosol surfaces. We estimate the forcing from biomass burning and non-biomass burning sources separately, as the contribution of anthropogenic activities to changes in biomass burning emissions remains uncertain (Heald et al., 2014). The average 2001–2015 simulated direct radiative forcing from fires is -0.011 $W\,m^{-2}$, which falls within the range of previous model assessments ($0.0 \pm 0.05 W\,m^{-2}$, (Myhre et al., 2013)) . In the following we focus on the radiative forcing from non-biomass burning sources from 1850 to 2001 and from 2001 to 2015.

4.1 Clear-sky aerosol direct radiative forcing

The aerosol clear-sky direct radiative forcing in 2001 relative to 1850 is -0.64 $W\,m^{-2}$, which agrees well with previous assessments (Table S4). This forcing is dominated by changes in sulfate (-0.73 $W\,m^{-2}$), which are partly offset by changes in BC (+0.36 $W\,m^{-2}$). Fig. 9c shows that the meridional distribution of the clear-sky radiative forcings of individual aerosols in 2001 relative to 1850 largely mirror that of their precursors' emissions. Some deviations can be noted however. For instance, the forcing from black carbon is enhanced at high latitudes because of the higher surface albedo (Myhre et al., 2013).

We find little change in the aerosol clear-sky direct radiative forcing in 2015 relative to 2001 (-0.04 $W\,m^{-2}$) consistent with previous studies (Murphy, 2013; Kühn et al., 2014). In AM3, this reflects the cancellation between the positive clear-sky aerosol direct radiative forcing in the northern midlatitudes (associated with the decrease of sulfate and the increase of BC) and the negative clear-sky aerosol direct radiative forcing in the northern tropics (associated with the increase of nitrate and sulfate aerosols).

Next we examine the sensitivity of individual forcings to anthropogenic emissions in both periods. The clear-sky direct radiative forcing of black carbon increases by 25% from 2001 to 2015, in good agreement with the change in BC emissions. In contrast, the clear-sky direct radiative forcing of sulfate changes little between 2001 and 2015 (+3%), while SO_2 emissions decline by -12.5% over the same time period. This small change in the sulfate forcing reflects the cancellation between opposite changes in the tropics, where the forcing from sulfate aerosols is negative, and the mid-

latitudes, where it is positive. AM3 shows a stronger sensitivity of the sulfate forcing to changes in SO_2 emissions in the tropics than in the midlatitudes. This difference can be attributed to regional differences in the oxidative environment, as a) greater actinic flux allows for more efficient oxidation of SO_2 in the tropics than in the midlatitudes (Fig. S4), and b) the efficiency of the oxidation of SO_2 to sulfate tends to increase with decreasing SO_2 emissions, as oxidant limitations become less important, which diminishes the sensitivity of sulfate to changes in SO_2 emissions in the midlatitudes (Fig. S4).

In contrast to sulfate, the change in the clear-sky direct radiative forcing from nitrate from 2001 to 2015 (+75%) is greater than the change in the emissions of its precursors (ammonia and NO emissions increase by less than 20%). The higher sensitivity of nitrate to emission changes in the 2001-2015 period is consistent with the decrease of sulfate in the northern midlatitudes, which enables more ammonia to react with nitric acid to produce ammonium nitrate (Ansari and Pandis, 1998). In the tropics, ammonia is less limiting (the ratio of ammonia to SO_2 emissions is higher) and the magnitude of both nitrate and sulfate forcings are simulated to increase from 2001 to 2015.

4.2 All-sky aerosol direct radiative forcing

Clouds can enhance the reflectivity of the surface beneath aerosols as well as mask the effect of aerosols underneath (Heald et al., 2014). Overall, clouds tend to amplify the forcing of absorbing aerosols and diminish that of scattering aerosols. The simulated aerosol forcing in 2001 is -0.09 $\mathrm{W\,m^{-2}}$, at the low end of previous multi-model assessments (-0.27 $\pm 0.15 \mathrm{W\,m^{-2}}$ (Myhre et al., 2013) and Table S4) switching sign from negative to positive North of $45°$. For comparison, the instantaneous radiative forcing from well-mixed greenhouse gases at TOA, as calculated from the GFDL Standalone radiation code (Schwarzkopf and Ramaswamy, 1999; Freidenreich and Ramaswamy, 1999), is +1.84 $\mathrm{W\,m^{-2}}$ in 2001.

From 2001 to 2015, the direct aerosol forcing is simulated to be +0.03 $\mathrm{W\,m^{-2}}$, including +0.12, -0.03, and -0.03 $\mathrm{W\,m^{-2}}$ from black carbon, sulfate, and nitrate, respectively. Myhre et al. (2017) recently reported a similar change in the overall direct radiative forcing (+0.01 $\mathrm{W\,m^{-2}}$) but different contributions from sulfate (+0.03 $\mathrm{W\,m^{-2}}$) and black carbon (+0.03 $\mathrm{W\,m^{-2}}$). Many factors could contribute to these differences including the radiative properties of aerosols (e.g., the mixing of sulfate with black carbon (Bond et al., 2013)) and the emission inventories. Further studies are needed to examine whether changes in the sensitivity of radiative forcing to anthropogenic emissions are robust across models. Such assessment would be especially important in the northern midlatitudes, where the direct radiative forcing from aerosols and greenhouse gases from 2001 to 2015 are simulated to be of similar magnitude (+0.25 $\mathrm{W\,m^{-2}}$).

5 Conclusions

We have derived estimates of the changes in the aerosol direct clear-sky shortwave radiative effect from 2001 to 2015 using variations in the outgoing shortwave clear-sky radiation from CERES-EBAF. Even over polluted regions, such changes can not be solely ascribed to aerosols and the impact of changes in surface albedo, water vapor and ozone on outgoing radiation need to be accounted for. In particular, we have shown that the effect of increasing anthropogenic aerosols on the outgoing radiation has been largely masked by a decrease in surface albedo over India.

We have used observed seasonal changes in AOD and aerosol effect over large source regions of anthropogenic emissions to assess the representation of anthropogenic emissions and their impact on atmospheric chemistry and the aerosol direct radiative effect in the GFDL-AM3 global chemistry-climate model. Such observational constraints may be especially valuable for future multi-model assessments.

Our work suggests a mature understanding of changes in the aerosol effect over the US and Europe, where the decrease of sulfate aerosols accounts for most of the increase (i.e., the weakening) in the aerosol direct clear-sky shortwave radiative effect. In contrast, the different mix of anthropogenic emissions in India and China results in a more complex speciation of aerosols responsible for changes in the aerosol direct effect, with large contributions from sulfate, nitrate, and black carbon. Trends in these regions remain challenging to capture in the GFDL AM3 model. Some of these biases may be model-specific, including the treatment of the mixing between sulfate and black carbon, the representation of the photochemistry of sulfate and nitrate, or the representation of dust emissions. Others are attributed to the CMIP6 emissions and will likely affect other models. In particular, we find that the model bias in winter over India can be largely accounted for by uncertainties in the seasonality of ammonia and black carbon emissions. Similarly, comparisons between the CMIP6 and MEIC emission inventories over China suggest that the model bias in this region can be largely attributed to an underestimate in CMIP6 of the reduction of SO_2 emissions after 2007.

Our study shows that regional differences in the emission mix and oxidative conditions have a large impact on the relationship between anthropogenic emissions and direct aerosol forcing. Specifically, we have shown that changes in the magnitude, speciation, and spatial distribution of anthropogenic emissions have dampened the sensitivity of the aerosol forcing to SO_2 emissions, but amplified that to emissions of NO and ammonia, the precursors of nitrate aerosols. This suggests that relationships between anthropogenic emissions and aerosol forcing derived over the 1850–2001 period and thus largely controlled by changes of SO_2 in Europe and North America (Stevens and Schwartz, 2012) need to be revisited with an emphasis on black carbon and ammonia in Asia.

Acknowledgements. We thank the many researchers, who have contributed to the CERES, MODIS, and MISR
products used in this study. CERES data were obtained from the NASA Langley Research Center CERES or-
dering tool at http://ceres.larc.nasa.gov/. MODIS albedo (MD43C3 MODIS/Terra+Aqua BRDF/Albedo Albedo
Daily L3 Global 0.05 Deg CMG V006) was obtained in netCDF file format from the Integrated Climate
Data Center (ICDC, http://icdc.cen.uni-hamburg.de, University of Hamburg, Hamburg, Germany). MISR and
MODIS AOD products can be obtained from the NASA Earthdata portal. Model outputs are available upon
request to Fabien.Paulot@noaa.gov. We thank Drs B. Zheng and Q. Zhang for providing MEIC gridded emis-
sions. This work was supported by NOAA Climate Program Office. P. G. acknowledges partial funding by
NASA through NNH14ZDA001N-ACMAP grant. We thanks Dr A. Jones, Dr. L.J. Donner, and two anony-
mous reviewers for helpful comments. All figures were generated using the NCAR Command Language (Ver-
sion 6.4.0, http://dx.doi.org/10.5065/D6WD3XH5).
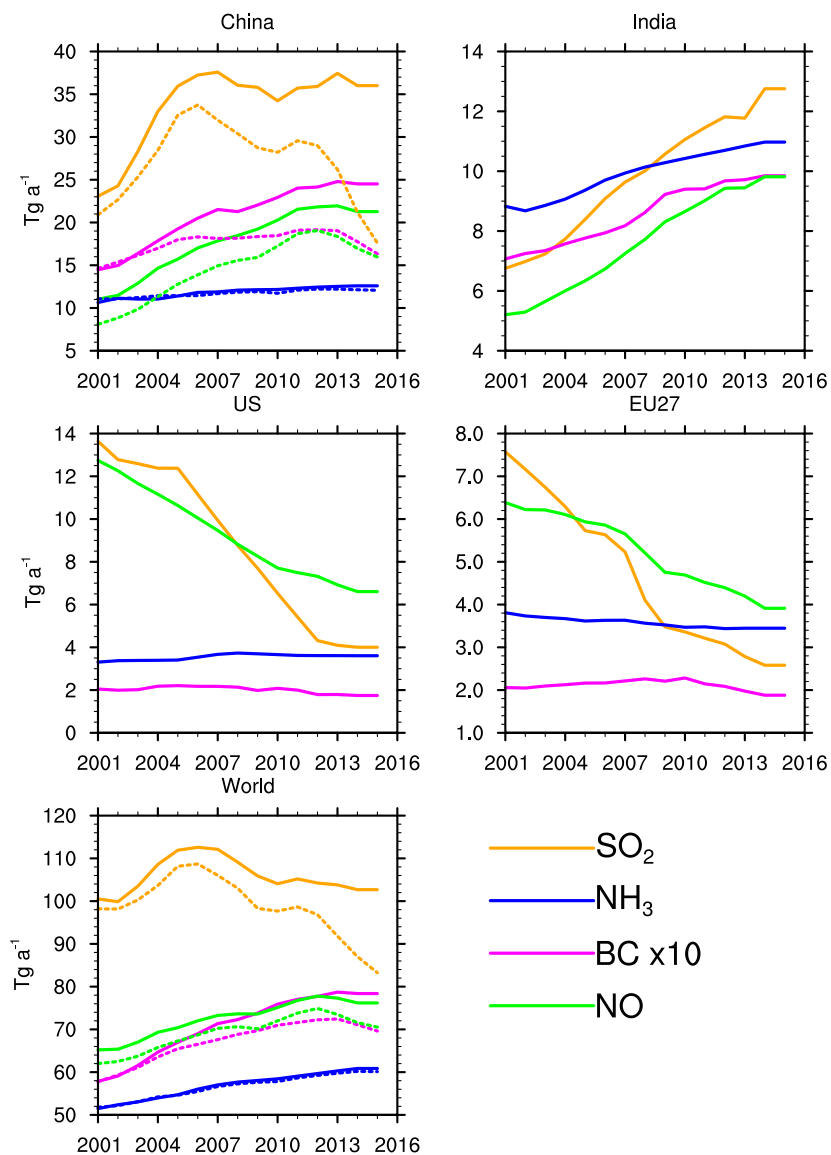
Figure 1. Annual anthropogenic emissions of SO_2, BC, NH_3, and NO from CMIP6 (solid lines) in selected regions. Emissions of SO_2, and NO with anthropogenic emissions from MEIC (for agriculture, energy, transportation, industry, and residential sectors) are also shown (dash lines).
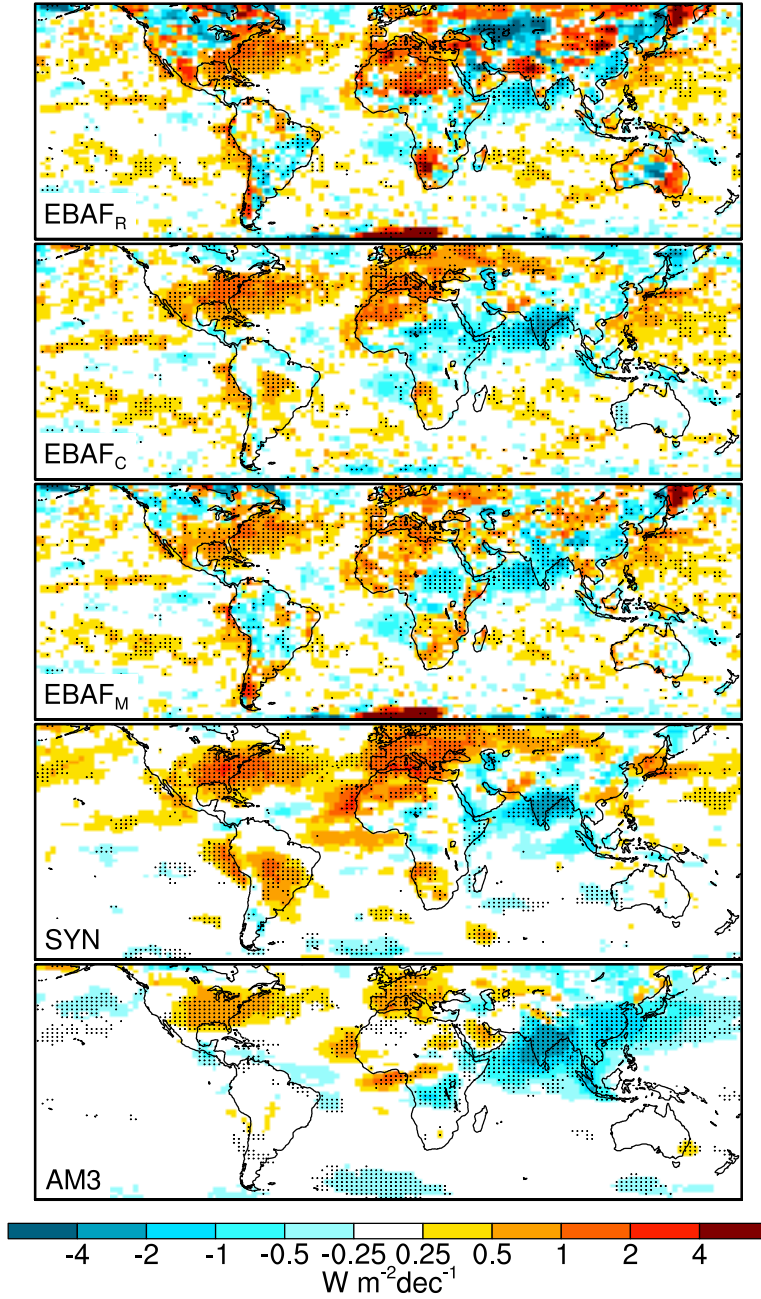
Figure 2. Rate of change in the clear-sky shortwave aerosol shortwave direct radiative effect (DRE_{clr}^{sw}). An increase in DRE_{clr}^{sw} reflects a decrease in the amount of radiation scattered to space by aerosols. $EBAF_R$ is based on the outgoing clear-sky shortwave radiation from CERES EBAF assuming its variability is solely associated with aerosols. $EBAF_C$ and $EBAF_M$ are estimated using the observed clear-sky outgoing shortwave fluxes from CERES EBAF after accounting for the variability of water vapor, ozone, and surface albedo from CERES-EBAF and MODIS, respectively. Estimates from SYN (calculation constrained by observations) and from the GFDL AM3 global chemistry-climate model are also shown. Dotted areas are significant at the 95% confidence level.
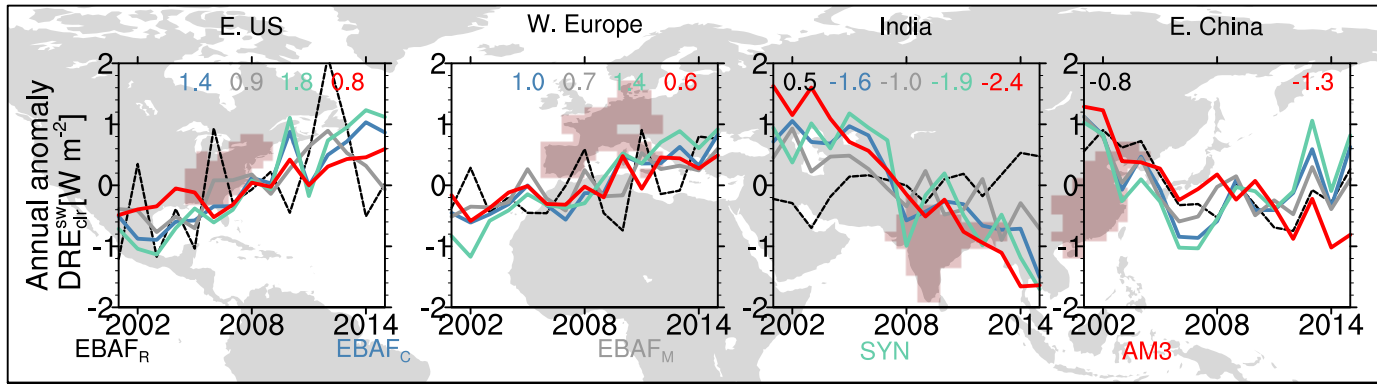
Figure 3. Regional changes in the clear-sky shortwave aerosol direct radiative effect derived from CERES-EBAF outgoing radiation without correction (EBAF$_R$ (black)) and after correcting for the variability of water, ozone, and surface albedo (from CERES-EBAF (EBAF$_C$, blue) or from MODIS (EBAF$_M$, grey)) over the Eastern US, Western Europe, India, and Eastern China. Estimates from SYN (calculation constrained by observations) and from the GFDL AM3 global chemistry-climate model are shown in green and red respectively. The rate of change for each estimate is indicated in $W\,m^{-2}\,decade^{-1}$ when significant (p<0.05).
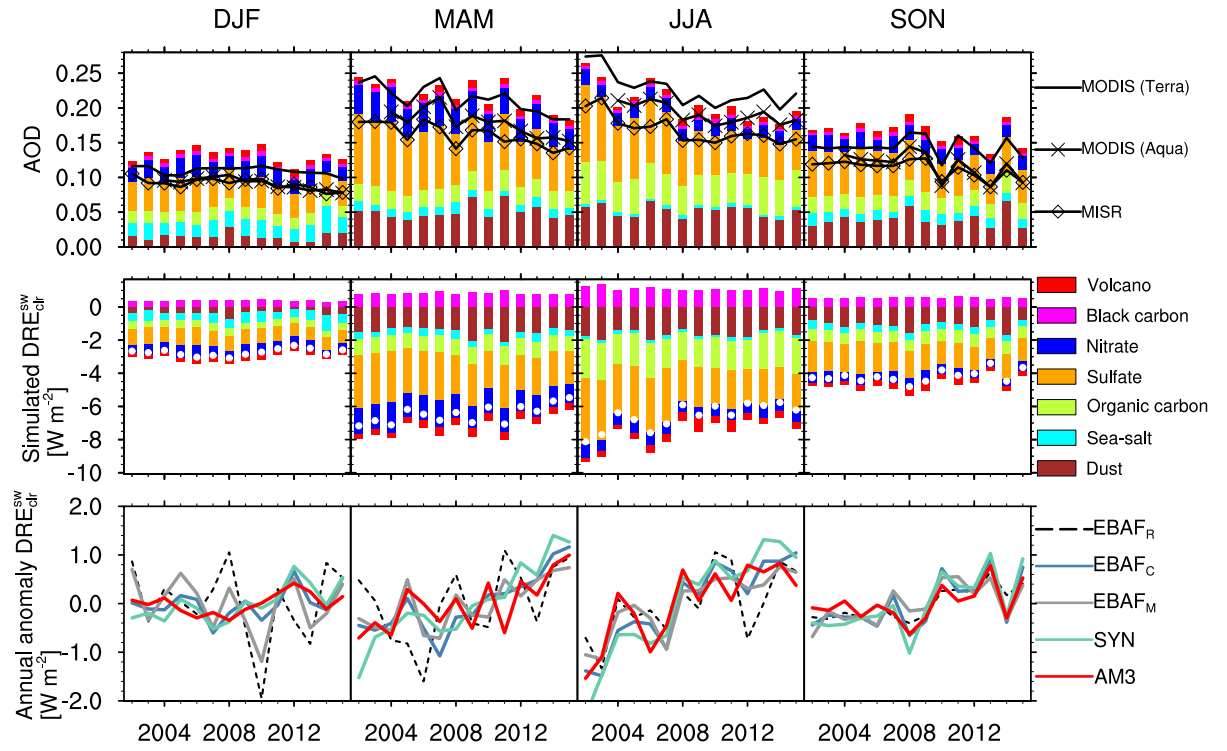
Figure 4. Seasonal changes in the aerosol optical depth (AOD) and clear-sky shortwave aerosol direct radiative effect (DRE_{clr}^{sw}) in Western Europe (Fig. 3). The top row shows the AOD retrieved from different spaceborne instruments (MODIS-Terra (lines), MODIS-Aqua (cross), MISR (diamond)) and the simulated AOD decomposed into its components (bars). The second row shows the simulated clear-sky shortwave aerosol direct radiative effect of individual aerosols (bars) and the overall aerosol direct radiative effect (white circle). The bottom row shows observation-based and simulated estimates of changes in the aerosol direct radiative effect.
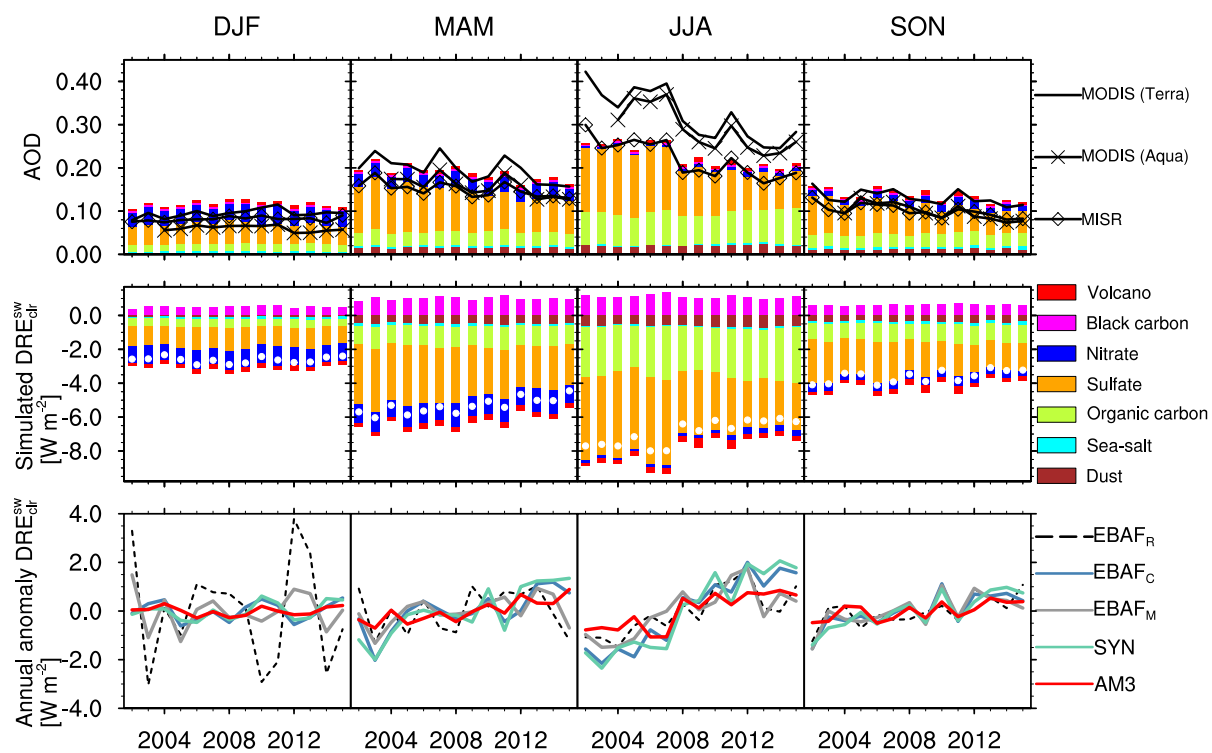
Figure 5. Same as 4 for the Eastern US
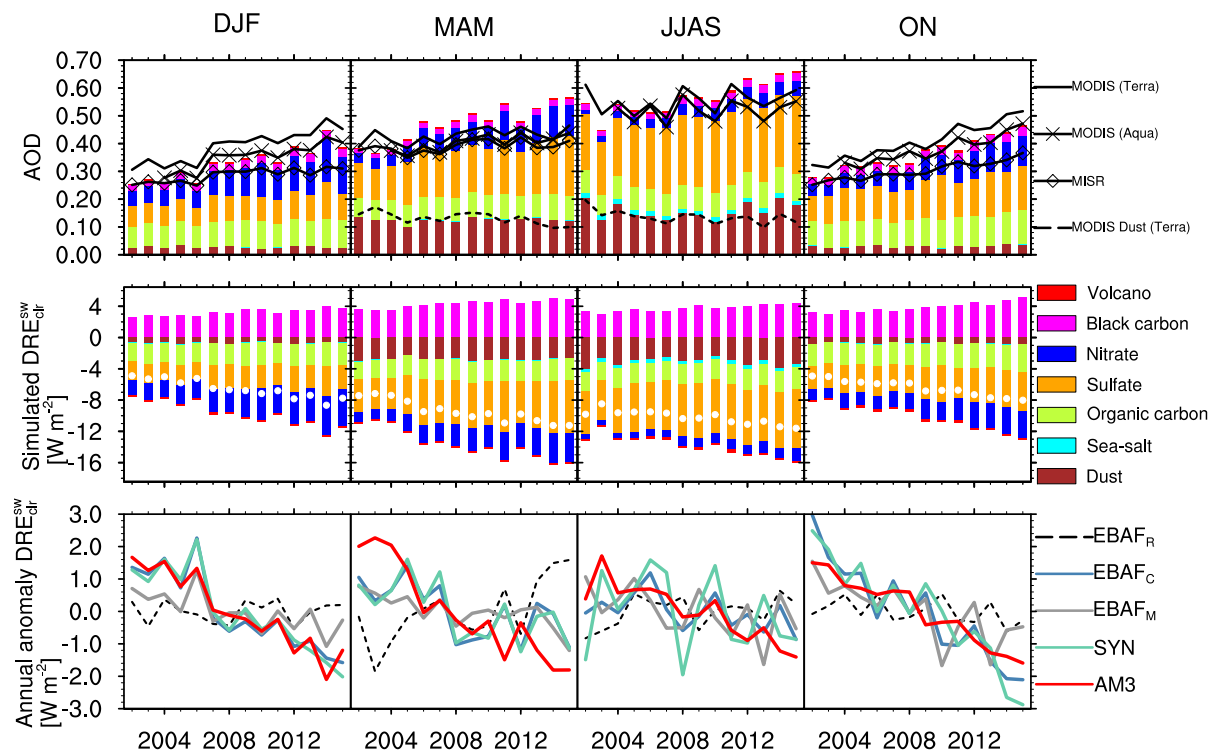
Figure 6. Same as 4 for the India. MISR is excluded in the monsoon season, when its coverage is too sparse relative to MODIS (TERRA). The MODIS-derived dust optical depth is indicated by a black dash line.
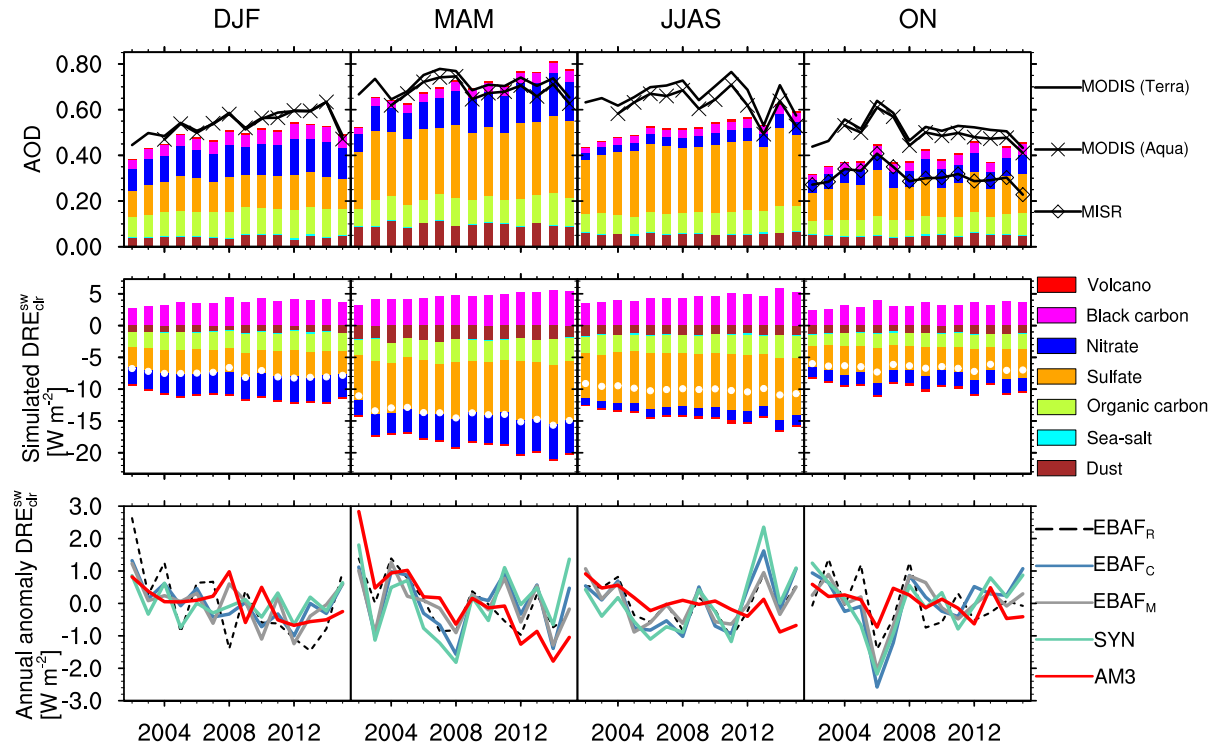
Figure 7. Same as 4 for Eastern China. MISR is excluded in winter, spring, and monsoon seasons, when its coverage is too sparse.
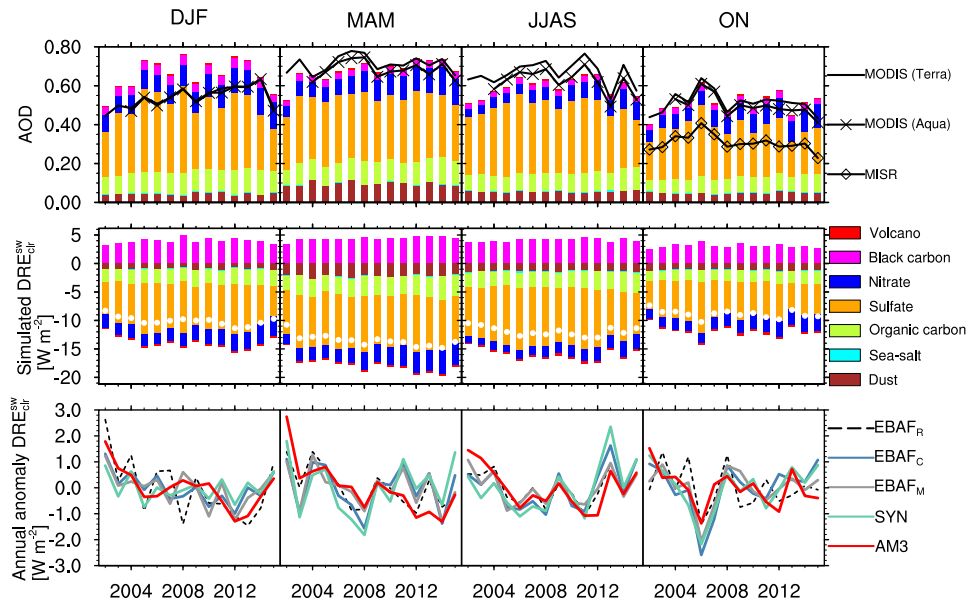
Figure 8. Same as Fig. 7 but including the heterogeneous oxidation of SO_2 and MEIC emissions over China (see text)
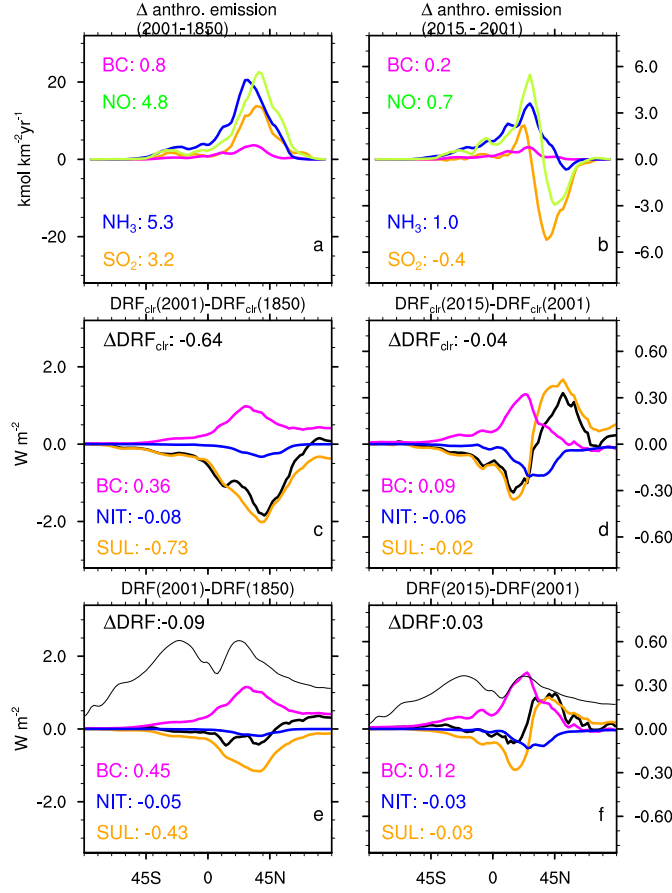
Figure 9. Meridional distribution of changes in anthropogenic emissions (BC, NO, NH_3, and SO_2) and in clear-sky (DRF_{clr}, middle row) and all-sky radiative aerosol direct radiative forcing (DRF, bottom row) from 1850 to 2001 (left) and from 2001 to 2015 (right). The thin black line indicates the instantaneous radiative forcing at TOA from well-mixed greenhouse gases. Global anthropogenic emissions and the total and speciated DRF_{clr} and DRF are indicated inline.

Table 1. Trends in the aerosol optical depth (AOD, decade^{-1}), and direct clear-sky shortwave radiative effect ($\mathrm{DRE_{clr}^{sw}}$, $\mathrm{W\,m^{-2}\,decade^{-1}}$) for selected regions and seasons from 2002 to 2015[a]

| | Western Europe | | Eastern US | | India | | Eastern China |
	MAM	JJA	MAM	JJA	DJF	MAM	MAM
AOD							
MODIS (TERRA)	-0.04 [0.21]	-0.04 [0.23]	-0.04 [0.20]	-0.11 [0.32]	0.13 [0.39]	0.04 [0.43]	* [0.71]
MODIS (AQUA)	-0.05 [0.18]	-0.03 [0.19]	-0.04 [0.16]	-0.10 [0.29]	0.11 [0.35]	0.07 [0.40]	* [0.68]
MISR	-0.03 [0.16]	-0.03 [0.17]	-0.02 [0.15]	-0.08 [0.22]	0.05 [0.29]	* [0.39]	
MATCH[b]	-0.06 [0.27]	-0.06 [0.26]	-0.07 [0.29]	-0.11 [0.35]	0.10 [0.36]	0.03 [0.49]	* [0.90]
AM3	-0.04 [0.22]	-0.05 [0.21]	-0.03 [0.19]	-0.05 [0.23]	0.13 [0.33]	0.15 [0.47]	0.15 [0.70]
sulfate	-0.03 [0.08]	-0.04 [0.07]	-0.03 [0.09]	-0.06 [0.12]	0.02 [0.09]	0.07 [0.17]	0.05 [0.30]
nitrate	-0.01 [0.04]	* [0.02]	* [0.03]	0.00 [0.01]	0.07 [0.10]	0.06 [0.07]	0.08 [0.14]
black carbon	* [0.01]	* [0.00]	* [0.01]	* [0.00]	0.01 [0.02]	0.01 [0.02]	0.01 [0.04]
$\mathrm{DRE_{clr}^{sw}}$							
SYN	1.8 [-8.9]	2.5 [-9.4]	2.1 [-8.6]	3.6 [-11.0]	-2.6 [-9.1]	-1.4 [-13.4]	* [-20.5]
$\mathrm{EBAF_C}$	1.4	1.8	1.3	3.3	-2.3	-1.2	*
$\mathrm{EBAF_M}$	1.0	1.2	*	2.0	-0.8	-0.9	*
AM3	1.1 [-6.5]	1.5 [-6.6]	0.9 [-5.3]	1.4 [-6.9]	-2.7 [-6.6]	-3.1 [-9.4]	-2.1 [-13.9]
sulfate	0.9 [-2.6]	1.5 [-2.7]	1.1 [-3.1]	2.2 [-3.9]	-0.7 [-2.9]	-1.8 [-5.5]	-1.1 [-8.5]
nitrate	0.3 [-1.4]	* [-0.7]	* [-1.2]	-0.2 [-0.2]	-2.4 [-3.3]	-1.9 [-2.6]	-2.2 [-4.2]
black carbon	* [0.8]	-0.2 [1.1]	* [1.0]	* [1.1]	0.9 [3.2]	1.2 [4.3]	1.4 [4.7]

[a] The average over the period 2002–2015 is shown in bracket (2003-2015 for AQUA). Trends are estimated using the Theil-Sen method. * denotes non significant monotonous change at $p = 0.05$. Model AOD is sampled based on MODIS (TERRA) seasonal coverage. No statistics is provided for China from MISR because of large differences in spatial coverage with MODIS (TERRA). SYN refers to the aerosol effect calculated in the CERES-SYN product. $\mathrm{EBAF_C}$ and $\mathrm{EBAF_M}$ refer to the aerosol effect estimated using CERES-EBAF outgoing shortwave clear-sky radiation corrected for the variability in water, ozone, and CERES-EBAF ($\mathrm{EBAF_C}$) and MODIS ($\mathrm{EBAF_M}$) surface albedo. Confidence intervals for the trends are provided in Table S2.

[b] from CERES-SYN Ed4 based on assimilation of MODIS Collection5 AOD with the MATCH model.

References

Alfaro-Contreras, R., Zhang, J., Reid, J. S., and Christopher, S.: A Study of the Longer Term Variation of Aerosol Optical Thickness and Direct Shortwave Aerosol Radiative Effect Trends Using MODIS and CERES, Atmos. Chem. Phys. Discuss., 2017, 1–63, doi:10.5194/acp-2017-365, https://www.atmos-chem-phys-discuss.net/acp-2017-365/, 2017.

Ansari, A. S. and Pandis, S. N.: Response of Inorganic PM to Precursor Concentrations, Environ. Sci. Technol., 32, 2706–2714, 1998.

Babu, S. S., Manoj, M. R., Moorthy, K. K., Gogoi, M. M., Nair, V. S., Kompalli, S. K., Satheesh, S. K., Niranjan, K., Ramagopal, K., Bhuyan, P. K., and Singh, D.: Trends in aerosol optical depth over Indian region: Potential causes and impact indicators, Journal of Geophysical Research: Atmospheres, 118, 2013JD020 507, doi:10.1002/2013JD020507, http://onlinelibrary.wiley.com/doi/10.1002/2013JD020507/abstract, 2013.

Bellouin, N., Boucher, O., Haywood, J., and Reddy, M. S.: Global estimate of aerosol direct radiative forcing from satellite measurements, Nature, 438, 1138–1141, doi:10.1038/nature04348, https://doi.org/10.1038/nature04348, 2005.

Bellouin, N., Jones, A., Haywood, J., and Christopher, S. A.: Updated estimate of aerosol direct radiative forcing from satellite observations and comparison against the Hadley Centre climate model, Journal of Geophysical Research: Atmospheres, 113, n/a–n/a, doi:10.1029/2007JD009385, http://dx.doi.org/10.1029/2007JD009385, d10205, 2008.

Bollasina, M. A., Ming, Y., and Ramaswamy, V.: Anthropogenic Aerosols and the Weakening of the South Asian Summer Monsoon, Science, 334, 502–505, doi:10.1126/science.1204994, http://science.sciencemag.org/content/334/6055/502, 2011.

Bond, T. C., Doherty, S. J., Fahey, D. W., Forster, P. M., Berntsen, T., DeAngelo, B. J., Flanner, M. G., Ghan, S., Kärcher, B., Koch, D., Kinne, S., Kondo, Y., Quinn, P. K., Sarofim, M. C., Schultz, M. G., Schulz, M., Venkataraman, C., Zhang, H., Zhang, S., Bellouin, N., Guttikunda, S. K., Hopke, P. K., Jacobson, M. Z., Kaiser, J. W., Klimont, Z., Lohmann, U., Schwarz, J. P., Shindell, D., Storelvmo, T., Warren, S. G., and Zender, C. S.: Bounding the role of black carbon in the climate system: A scientific assessment, Journal of Geophysical Research: Atmospheres, 118, 5380–5552, doi:10.1002/jgrd.50171, http://dx.doi.org/10.1002/jgrd.50171, 2013.

Boucher, O., Randall, D., Artaxo, P., Bretherton, C., Feingold, G., Forster, P., Kerminen, V.-M., Kondo, Y., Liao, H., Lohmann, U., Rasch, P., Satheesh, S., Sherwood, S., Stevens, B., and Zhang, X.: Clouds and Aerosols, book section 7, pp. 571–658, Cambridge University Press, Cambridge, United Kingdom and New York, NY, USA, doi:10.1017/CBO9781107415324.016, www.climatechange2013.org, 2013.

Cescatti, A., Marcolla, B., Santhana Vannan, S. K., Pan, J. Y., Román, M. O., Yang, X., Ciais, P., Cook, R. B., Law, B. E., Matteucci, G., Migliavacca, M., Moors, E., Richardson, A. D., Seufert, G., and Schaaf, C. B.: Intercomparison of MODIS albedo retrievals and in situ measurements across the global FLUXNET network, Remote Sens. Environ., 121, 323–334, doi:10.1016/j.rse.2012.02.019, http://www.sciencedirect.com/science/article/pii/S0034425712001125, 2012.

Charlson, R. J., Schwartz, S. E., Hales, J. M., Cess, R. D., Coakley, J. A., Hansen, J. E., and Hofmann, D. J.: Climate Forcing by Anthropogenic Aerosols, Science, 255, 423–430, doi:10.1126/science.255.5043.423, http://science.sciencemag.org/content/255/5043/423, 1992.

525   Cheng, Y., Zheng, G., Wei, C., Mu, Q., Zheng, B., Wang, Z., Gao, M., Zhang, Q., He, K., Carmichael, G., schl, U. P., and Su, H.: Reactive nitrogen chemistry in aerosol water as a source of sulfate during haze events in China, Sci. Adv., 2, e1601 530–e1601 530, doi:10.1126/sciadv.1601530, https://doi.org/10.1126/sciadv.1601530, 2016.

Christopher, S. A. and Zhang, J.: Cloud-free shortwave aerosol radiative effect over oceans: Strategies for
530   identifying anthropogenic forcing from Terra satellite measurements, Geophys. Res. Lett., 31, n/a–n/a, doi:10.1029/2004GL020510, http://dx.doi.org/10.1029/2004GL020510, 118101, 2004.

CMIP6 Data Request: Data Request Section: CMORvar, http://clipc-services.ceda.ac.uk/dreq/index/CMORvar.html, 2018.

Collins, W. D., Rasch, P. J., Eaton, B. E., Khattatov, B. V., Lamarque, J.-F., and Zender, C. S.: Simulating
535   aerosols using a chemical transport model with assimilation of satellite aerosol retrievals: Methodology for INDOEX, Journal of Geophysical Research: Atmospheres, 106, 7313–7336, doi:10.1029/2000JD900507, http://onlinelibrary.wiley.com/doi/10.1029/2000JD900507/abstract, 2001.

de Foy, B., Lu, Z., and Streets, D. G.: Satellite NO2 retrievals suggest China has exceeded its NOx reduction goals from the twelfth Five-Year Plan, Sci. Rep., 6, doi:10.1038/srep35912, https://www.ncbi.nlm.nih.gov/
540   pmc/articles/PMC5082360/, 2016.

Dentener, F., Kinne, S., Bond, T., Boucher, O., Cofala, J., Generoso, S., Ginoux, P., Gong, S., Hoelzemann, J. J., Ito, A., Marelli, L., Penner, J. E., Putaud, J.-P., Textor, C., Schulz, M., van der Werf, G. R., and Wilson, J.: Emissions of primary aerosol and precursor gases in the years 2000 and 1750 prescribed data-sets for AeroCom, Atmos. Chem. Phys., 6, 4321–4344, doi:10.5194/acp-6-4321-2006, https://doi.org/10.5194/
545   acp-6-4321-2006, 2006.

Ding, J., Miyazaki, K., van der A, R. J., Mijling, B., Kurokawa, J.-I., Cho, S., Janssens-Maenhout, G., Zhang, Q., Liu, F., and Levelt, P. F.: Intercomparison of NOx emission inventories over East Asia, Atmos. Chem. Phys., 17, 10 125–10 141, doi:10.5194/acp-17-10125-2017, https://www.atmos-chem-phys.net/17/10125/2017/, 2017.

550   Donner, L. J., Wyman, B. L., Hemler, R. S., Horowitz, L. W., Ming, Y., Zhao, M., Golaz, J.-C., Ginoux, P., Lin, S.-J., Schwarzkopf, M. D., Austin, J., Alaka, G., Cooke, W. F., Delworth, T. L., Freidenreich, S. M., Gordon, C. T., Griffies, S. M., Held, I. M., Hurlin, W. J., Klein, S. A., Knutson, T. R., Langenhorst, A. R., Lee, H.-C., Lin, Y., Magi, B. I., Malyshev, S. L., Milly, P. C. D., Naik, V., Nath, M. J., Pincus, R., Ploshay, J. J., Ramaswamy, V., Seman, C. J., Shevliakova, E., Sirutis, J. J., Stern, W. F., Stouffer, R. J., Wilson, R. J.,
555   Winton, M., Wittenberg, A. T., and Zeng, F.: The Dynamical Core, Physical Parameterizations, and Basic Simulation Characteristics of the Atmospheric Component AM3 of the GFDL Global Coupled Model CM3, J. Clim., 24, 3484–3519, 2011.

Freidenreich, S. M. and Ramaswamy, V.: A new multiple-band solar radiative parameterization for general circulation models, Journal of Geophysical Research: Atmospheres, 104, 31 389–31 409,
560   doi:10.1029/1999jd900456, https://doi.org/10.1029/1999jd900456, 1999.

Ginoux, P., Prospero, J. M., Gill, T. E., Hsu, N. C., and Zhao, M.: Global-scale attribution of anthropogenic and natural dust sources and their emission rates based on MODIS Deep Blue aerosol products, Rev. Geophys., 50, RG3005, 2012.

Griffies, S. M., Winton, M., Donner, L. J., Horowitz, L. W., Downes, S. M., Farneti, R., Gnanadesikan, A., Hurlin, W. J., Lee, H.-C., Liang, Z., Palter, J. B., Samuels, B. L., Wittenberg, A. T., Wyman, B. L., Yin, J., and Zadeh, N.: The GFDL CM3 Coupled Climate Model: Characteristics of the Ocean and Sea Ice Simulations, J. Clim., 24, 3520–3544, doi:10.1175/2011JCLI3964.1, http://journals.ametsoc.org/doi/abs/10.1175/2011JCLI3964.1, 2011.

Guenther, A., Karl, T., Harley, P., Wiedinmyer, C., Palmer, P. I., and Geron, C.: Estimates of global terrestrial isoprene emissions using MEGAN (Model of Emissions of Gases and Aerosols from Nature), Atmos. Chem. Phys., 6, 3181–3210, 2006.

Guo, H., Weber, R. J., and Nenes, A.: High levels of ammonia do not raise fine particle pH sufficiently to yield nitrogen oxide-dominated sulfate production, Sci. Rep., 7, doi:10.1038/s41598-017-11704-0, https://doi.org/10.1038/s41598-017-11704-0, 2017.

He, P., Alexander, B., Geng, L., Chi, X., Fan, S., Zhan, H., Kang, H., Zheng, G., Cheng, Y., Su, H., Liu, C., and Xie, Z.: Isotopic constraints on heterogeneous sulphate production in Beijing haze, Atmos. Chem. Phys. Discuss., pp. 1–25, doi:10.5194/acp-2017-977, https://doi.org/10.5194/acp-2017-977, 2017.

Heald, C. L., Collett, J. L., Lee, T., Benedict, K. B., Schwandner, F. M., Li, Y., Clarisse, L., Hurtmans, D. R., Van Damme, M., Clerbaux, C., Coheur, P.-F., and Pye, H. O. T.: Atmospheric ammonia and particulate inorganic nitrogen over the United States, Atmos. Chem. Phys., 12, 10 295–10 312, 2012.

Heald, C. L., Ridley, D. A., Kroll, J. H., Barrett, S. R. H., Cady-Pereira, K. E., Alvarado, M. J., and Holmes, C. D.: Contrasting the direct radiative effect and direct radiative forcing of aerosols, Atmos. Chem. Phys., 14, 5513–5527, doi:10.5194/acp-14-5513-2014, http://www.atmos-chem-phys.net/14/5513/2014/, 2014.

Hoesly, R. M., Smith, S. J., Feng, L., Klimont, Z., Janssens-Maenhout, G., Pitkanen, T., Seibert, J. J., Vu, L., Andres, R. J., Bolt, R. M., Bond, T. C., Dawidowski, L., Kholod, N., Kurokawa, J.-I., Li, M., Liu, L., Lu, Z., Moura, M. C. P., O'Rourke, . P. R., and Zhang, Q.: Historical (1750–2014) anthropogenic emissions of reactive gases and aerosols from the Community Emissions Data System (CEDS), Geosci. Model Dev., 11, 369–408, doi:10.5194/gmd-11-369-2018, https://www.geosci-model-dev.net/11/369/2018/, 2018.

Hung, H.-M. and Hoffmann, M. R.: Oxidation of gas-phase SO_2 on the surfaces of acidic microdroplets: implications for sulfate and sulfate radical anion formation in the atmospheric liquid phase, Environ. Sci. Technol., 49, 13 768–13 776, doi:10.1021/acs.est.5b01658, http://dx.doi.org/10.1021/acs.est.5b01658, 2015.

Irie, H., Muto, T., Itahashi, S., Kurokawa, J.-i., and Uno, I.: Turnaround of Tropospheric Nitrogen Dioxide Pollution Trends in China, Japan, and South Korea, Sola, 12, 170–174, doi:10.2151/sola.2016-035, 2016.

Jin, Q. and Wang, C.: The greening of Northwest Indian subcontinent and reduction of dust abundance resulting from Indian summer monsoon revival, Scientific Reports, 8, doi:10.1038/s41598-018-23055-5, https://doi.org/10.1038/s41598-018-23055-5, 2018.

John, J. G., Fiore, A. M., Naik, V., Horowitz, L. W., and Dunne, J. P.: Climate versus emission drivers of methane lifetime against loss by tropospheric OH from 1860–2100, Atmos. Chem. Phys., 12, 12 021–12 036, 2012.

Kahn, R. A.: Reducing the Uncertainties in Direct Aerosol Radiative Forcing, Surv. Geophys., 33, 701–721, doi:10.1007/s10712-011-9153-z, https://link.springer.com/article/10.1007/s10712-011-9153-z, 2012.

Kahn, R. A., Gaitley, B. J., Martonchik, J. V., Diner, D. J., Crean, K. A., and Holben, B.: Multiangle Imaging Spectroradiometer (MISR) global aerosol optical depth validation based on 2 years of coincident Aerosol

Robotic Network (AERONET) observations, Journal of Geophysical Research: Atmospheres, 110, n/a–n/a, doi:10.1029/2004JD004706, http://dx.doi.org/10.1029/2004JD004706, d10S04, 2005.

605   Kahn, R. A., Gaitley, B. J., Garay, M. J., Diner, D. J., Eck, T. F., Smirnov, A., and Holben, B. N.: Multiangle Imaging SpectroRadiometer global aerosol product assessment by comparison with the Aerosol Robotic Network, Journal of Geophysical Research: Atmospheres, 115, n/a–n/a, doi:10.1029/2010JD014601, http://dx.doi.org/10.1029/2010JD014601, d23209, 2010.

Kalnay, E., Kanamitsu, M., Kistler, R., Collins, W., Deaven, D., Gandin, L., Iredell, M., Saha, S., White, G.,
610   Woollen, J., Zhu, Y., Leetmaa, A., Reynolds, R., Chelliah, M., Ebisuzaki, W., Higgins, W., Janowiak, J., Mo, K. C., Ropelewski, C., Wang, J., Jenne, R., and Joseph, D.: The NCEP/NCAR 40-Year Reanalysis Project, Bull. Am. Meteorol. Soc., 77, 437–471, 1996.

Kendall, M. G.: A new measure of rank correlation, Biometrika, 30, 81–93, doi:10.1093/biomet/30.1-2.81, +http://dx.doi.org/10.1093/biomet/30.1-2.81, 1938.

615   Kim, D., Chin, M., Bian, H., Tan, Q., Brown, M. E., Zheng, T., You, R., Diehl, T., Ginoux, P., and Kucsera, T.: The effect of the dynamic surface bareness on dust source function, emission, and distribution, Journal of Geophysical Research: Atmospheres, 118, 871–886, doi:10.1029/2012JD017907, http://onlinelibrary.wiley.com/doi/10.1029/2012JD017907/abstract, 2013.

Krotkov, N. A., McLinden, C. A., Li, C., Lamsal, L. N., Celarier, E. A., Marchenko, S. V., Swartz, W. H.,
620   Bucsela, E. J., Joiner, J., Duncan, B. N., Boersma, K. F., Veefkind, J. P., Levelt, P. F., Fioletov, V. E., Dickerson, R. R., He, H., Lu, Z., and Streets, D. G.: Aura OMI observations of regional SO2 and NO2 pollution changes from 2005 to 2015, Atmos. Chem. Phys., 16, 4605–4629, doi:10.5194/acp-16-4605-2016, https://www.atmos-chem-phys.net/16/4605/2016/, 2016.

Kühn, T., Partanen, A.-I., Laakso, A., Lu, Z., Bergman, T., Mikkonen, S., Kokkola, H., Korhonen, H., Räisä-
625   nen, P., Streets, D. G., Romakkaniemi, S., and Laaksonen, A.: Climate impacts of changing aerosol emissions since 1996, Geophys. Res. Lett., 41, 4711–4718, doi:10.1002/2014gl060349, https://doi.org/10.1002/2014gl060349, 2014.

Levy, H., Horowitz, L. W., Schwarzkopf, M. D., Ming, Y., Golaz, J.-C., Naik, V., and Ramaswamy, V.: The roles of aerosol direct and indirect effects in past and future climate change, J. Geophys. Res. Atmos., 118,
630   4521–4532, 2013a.

Levy, R. C., Remer, L. A., Kleidman, R. G., Mattoo, S., Ichoku, C., Kahn, R., and Eck, T. F.: Global evaluation of the Collection 5 MODIS dark-target aerosol products over land, Atmos. Chem. Phys., 10, 10 399–10 420, doi:10.5194/acp-10-10399-2010, https://www.atmos-chem-phys.net/10/10399/2010/, 2010.

Levy, R. C., Mattoo, S., Munchak, L. A., Remer, L. A., Sayer, A. M., Patadia, F., and Hsu, N. C.: The Collection
635   6 MODIS aerosol products over land and ocean, Atmos. Meas. Tech., 6, 2989–3034, doi:10.5194/amt-6-2989-2013, https://doi.org/10.5194/amt-6-2989-2013, 2013b.

Li, C., Zhang, Q., Krotkov, N. A., Streets, D. G., He, K., Tsay, S.-C., and Gleason, J. F.: Recent large reduction in sulfur dioxide emissions from Chinese power plants observed by the Ozone Monitoring Instrument, Geophys. Res. Lett., 37, n/a–n/a, doi:10.1029/2010GL042594, http://dx.doi.org/10.1029/2010GL042594,
640   l08807, 2010.

Liu, F., Zhang, Q., A, R. J. v. d., Zheng, B., Tong, D., Yan, L., Zheng, Y., and He, K.: Recent reduction in NO
  x emissions over China: synthesis of satellite observations and emission inventories, Environ. Res. Lett., 11,
  114 002, doi:10.1088/1748-9326/11/11/114002, http://stacks.iop.org/1748-9326/11/i=11/a=114002, 2016.

Loeb, N. G. and Manalo-Smith, N.: Top-of-Atmosphere Direct Radiative Effect of Aerosols over Global Oceans
645   from Merged CERES and MODIS Observations, J. Climate, 18, 3506–3526, doi:10.1175/JCLI3504.1, http:
  //journals.ametsoc.org/doi/abs/10.1175/JCLI3504.1, 2005.

Loeb, N. G., Doelling, D. R., Wang, H., Su, W., Nguyen, C., Corbett, J. G., Liang, L., Mitrescu, C., Rose, F. G.,
  and Kato, S.: Clouds and the Earth's Radiant Energy System (CERES) Energy Balanced and Filled (EBAF)
  Top-of-Atmosphere (TOA) Edition-4.0 Data Product, Journal of Climate, 31, 895–918, doi:10.1175/jcli-d-
650   17-0208.1, https://doi.org/10.1175/jcli-d-17-0208.1, 2018.

Murphy, D. M.: Little net clear-sky radiative forcing from recent regional redistribution of aerosols, Nat.
  Geosci., 6, 258–262, doi:10.1038/ngeo1740, https://doi.org/10.1038/ngeo1740, 2013.

Myhre, G., Samset, B. H., Schulz, M., Balkanski, Y., Bauer, S., Berntsen, T. K., Bian, H., Bellouin, N., Chin,
  M., Diehl, T., Easter, R. C., Feichter, J., Ghan, S. J., Hauglustaine, D., Iversen, T., Kinne, S., Kirkevåg, A.,
655   Lamarque, J.-F., Lin, G., Liu, X., Lund, M. T., Luo, G., Ma, X., van Noije, T., Penner, J. E., Rasch, P. J.,
  Ruiz, A., Seland, Ø., Skeie, R. B., Stier, P., Takemura, T., Tsigaridis, K., Wang, P., Wang, Z., Xu, L., Yu, H.,
  Yu, F., Yoon, J.-H., Zhang, K., Zhang, H., and Zhou, C.: Radiative forcing of the direct aerosol effect from
  AeroCom Phase II simulations, Atmos. Chem. Phys., 13, 1853–1877, 2013.

Myhre, G., Aas, W., Cherian, R., Collins, W., Faluvegi, G., Flanner, M., Forster, P., Hodnebrog, Ø., Klimont, Z.,
660   Lund, M. T., Mülmenstädt, J., Lund Myhre, C., Olivié, D., Prather, M., Quaas, J., Samset, B. H., Schnell, J. L.,
  Schulz, M., Shindell, D., Skeie, R. B., Takemura, T., and Tsyro, S.: Multi-model simulations of aerosol and
  ozone radiative forcing due to anthropogenic emission changes during the period 1990–2015, Atmospheric
  Chemistry and Physics, 17, 2709–2720, doi:10.5194/acp-17-2709-2017, https://www.atmos-chem-phys.net/
  17/2709/2017/, 2017.

665 Naik, V., Horowitz, L. W., Fiore, A. M., Ginoux, P., Mao, J., Aghedo, A. M., and Levy, H.: Impact of prein-
  dustrial to present-day changes in short-lived pollutant emissions on atmospheric composition and climate
  forcing, J. Geophys. Res. Atmos., 118, 8086–8110, 2013.

Pan, X., Chin, M., Gautam, R., Bian, H., Kim, D., Colarco, P. R., Diehl, T. L., Takemura, T., Pozzoli, L.,
  Tsigaridis, K., Bauer, S., and Bellouin, N.: A multi-model evaluation of aerosols over South Asia: common
670   problems and possible causes, Atmos. Chem. Phys., 15, 5903–5928, doi:10.5194/acp-15-5903-2015, https:
  //www.atmos-chem-phys.net/15/5903/2015/, 2015.

Patadia, F., Gupta, P., and Christopher, S. A.: First observational estimates of global clear sky shortwave
  aerosol direct radiative effect over land, Geophys. Res. Lett., 35, L04 810, doi:10.1029/2007GL032314,
  http://onlinelibrary.wiley.com/doi/10.1029/2007GL032314/abstract, 2008.

675 Paulot, F., Jacob, D. J., Pinder, R. W., Bash, J. O., Travis, K., and Henze, D. K.: Ammonia emissions in the
  United States, European Union, and China derived by high-resolution inversion of ammonium wet deposition
  data: Interpretation with a new agricultural emissions inventory (MASAGE_NH3), J. Geophys. Res. Atmos.,
  119, 4343–4364, 2014.

Paulot, F., Ginoux, P., Cooke, W. F., Donner, L. J., Fan, S., Lin, M.-Y., Mao, J., Naik, V., and Horowitz, L. W.:
680   Sensitivity of nitrate aerosols to ammonia emissions and to nitrate chemistry: implications for present and

future nitrate optical depth, Atmos. Chem. Phys., 16, 1459–1477, doi:10.5194/acp-16-1459-2016, http://www.atmos-chem-phys.net/16/1459/2016/, 2016.

Paulot, F., Fan, S., and Horowitz, L. W.: Contrasting seasonal responses of sulfate aerosols to declining SO_2 emissions in the Eastern U.S.: Implications for the efficacy of SO_2 emission controls, Geophys. Res. Lett., 44,
685   455–464, doi:10.1002/2016GL070695, http://dx.doi.org/10.1002/2016GL070695, 2016GL070695, 2017a.

Paulot, F., Paynter, D., Ginoux, P., Naik, V., Whitburn, S., Van Damme, M., Clarisse, L., Coheur, P.-F., and Horowitz, L. W.: Gas-aerosol partitioning of ammonia in biomass burning plumes: Implications for the interpretation of spaceborne observations of ammonia and the radiative forcing of ammonium nitrate, Geophys. Res. Lett., 44, 2017GL074 215, doi:10.1002/2017GL074215, http://onlinelibrary.wiley.com/doi/10.
690   1002/2017GL074215/abstract, 2017b.

Rayner, N. A., Parker, D. E., Horton, E. B., Folland, C. K., Alexander, L. V., Rowell, D. P., Kent, E. C., and Kaplan, A.: Global analyses of sea surface temperature, sea ice, and night marine air temperature since the late nineteenth century, J. Geophys. Res. Atmos., 108, 4407, doi:10.1029/2002JD002670, http://dx.doi.org/10.1029/2002JD002670, 2003.

695 Rosenfeld, D., Andreae, M. O., Asmi, A., Chin, M., de Leeuw, G., Donovan, D. P., Kahn, R., Kinne, S., Kivekäs, N., Kulmala, M., Lau, W., Schmidt, K. S., Suni, T., Wagner, T., Wild, M., and Quaas, J.: Global observations of aerosol-cloud-precipitation-climate interactions, Rev. Geophys., 52, 2013RG000 441, doi:10.1002/2013RG000441, http://onlinelibrary.wiley.com/doi/10.1002/2013RG000441/abstract, 2014.

Rutan, D., Rose, F., Roman, M., Manalo-Smith, N., Schaaf, C., and Charlock, T.: Development and as-
700   sessment of broadband surface albedo from Clouds and the Earth's Radiant Energy System Clouds and Radiation Swath data product, Journal of Geophysical Research: Atmospheres, 114, D08 125, doi:10.1029/2008JD010669, http://onlinelibrary.wiley.com/doi/10.1029/2008JD010669/abstract, 2009.

Rutan, D. A., Kato, S., Doelling, D. R., Rose, F. G., Nguyen, L. T., Caldwell, T. E., and Loeb, N. G.: CERES Synoptic Product: Methodology and Validation of Surface Radiant Flux, J. Atmos. Oceanic
705   Technol., 32, 1121–1143, doi:10.1175/JTECH-D-14-00165.1, http://journals.ametsoc.org/doi/abs/10.1175/JTECH-D-14-00165.1, 2015.

Saikawa, E., Kim, H., Zhong, M., Avramov, A., Zhao, Y., Janssens-Maenhout, G., ichi Kurokawa, J., Klimont, Z., Wagner, F., Naik, V., Horowitz, L. W., and Zhang, Q.: Comparison of emissions inventories of anthropogenic air pollutants and greenhouse gases in China, Atmospheric Chemistry and Physics, 17, 6393–6421,
710   doi:10.5194/acp-17-6393-2017, https://doi.org/10.5194/acp-17-6393-2017, 2017a.

Saikawa, E., Trail, M., Zhong, M., Wu, Q., Young, C. L., Janssens-Maenhout, G., Klimont, Z., Wagner, F., ichi Kurokawa, J., Nagpure, A. S., and Gurjar, B. R.: Uncertainties in emissions estimates of greenhouse gases and air pollutants in India and their impacts on regional air quality, Environmental Research Letters, 12, 065 002, doi:10.1088/1748-9326/aa6cb4, https://doi.org/10.1088/1748-9326/aa6cb4, 2017b.

715 Sayer, A. M., Munchak, L. A., Hsu, N. C., Levy, R. C., Bettenhausen, C., and Jeong, M.-J.: MODIS Collection 6 aerosol products: Comparison between Aqua's e-Deep Blue, Dark Target, and "merged" data sets, and usage recommendations, Journal of Geophysical Research: Atmospheres, 119, 13,965–13,989, doi:10.1002/2014JD022453, http://dx.doi.org/10.1002/2014JD022453, 2014JD022453, 2014.

Schaaf, C. B., Gao, F., Strahler, A. H., Lucht, W., Li, X., Tsang, T., Strugnell, N. C., Zhang, X., Jin, Y.,
720   Muller, J.-P., Lewis, P., Barnsley, M., Hobson, P., Disney, M., Roberts, G., Dunderdale, M., Doll, C.,

d'Entremont, R. P., Hu, B., Liang, S., Privette, J. L., and Roy, D.: First operational BRDF, albedo nadir reflectance products from MODIS, Remote Sens. Environ., 83, 135–148, doi:10.1016/S0034-4257(02)00091-3, http://www.sciencedirect.com/science/article/pii/S0034425702000913, 2002.

Schwarzkopf, M. D. and Ramaswamy, V.: Radiative effects of CH4, N2O, halocarbons and the foreign-broadened H2O continuum: A GCM experiment, Journal of Geophysical Research: Atmospheres, 104, 9467–9488, doi:10.1029/1999jd900003, https://doi.org/10.1029/1999jd900003, 1999.

Sen, P. K.: Estimates of the Regression Coefficient Based on Kendall's Tau, J. Am. Stat. Assoc., 63, 1379–1389, doi:10.1080/01621459.1968.10480934, http://www.tandfonline.com/doi/abs/10.1080/01621459.1968.10480934, 1968.

Shell, K. M., Kiehl, J. T., and Shields, C. A.: Using the Radiative Kernel Technique to Calculate Climate Feedbacks in NCAR's Community Atmospheric Model, Journal of Climate, 21, 2269–2282, doi:10.1175/2007jcli2044.1, https://doi.org/10.1175/2007jcli2044.1, 2008.

Soden, B. J., Held, I. M., Colman, R., Shell, K. M., Kiehl, J. T., and Shields, C. A.: Quantifying Climate Feedbacks Using Radiative Kernels, Journal of Climate, 21, 3504–3520, doi:10.1175/2007jcli2110.1, https://doi.org/10.1175/2007jcli2110.1, 2008.

Stevens, B.: Rethinking the Lower Bound on Aerosol Radiative Forcing, J. Climate, 28, 4794–4819, doi:10.1175/JCLI-D-14-00656.1, https://doi.org/10.1175/JCLI-D-14-00656.1, 2015.

Stevens, B. and Schwartz, S. E.: Observing and Modeling Earth's Energy Flows, Surv. Geophys., 33, 779–816, doi:10.1007/s10712-012-9184-0, https://doi.org/10.1007/s10712-012-9184-0, 2012.

Stevens, B., Fiedler, S., Kinne, S., Peters, K., Rast, S., Müsse, J., Smith, S. J., and Mauritsen, T.: MACv2-SP: a parameterization of anthropogenic aerosol optical properties and an associated Twomey effect for use in CMIP6, Geosci. Model Dev., 10, 433–452, doi:10.5194/gmd-10-433-2017, https://www.geosci-model-dev.net/10/433/2017/, 2017.

Storelvmo, T., Leirvik, T., Lohmann, U., Phillips, P. C. B., and Wild, M.: Disentangling greenhouse warming and aerosol cooling to reveal Earth's climate sensitivity, Nat. Geosci., 9, 286–289, doi:10.1038/ngeo2670, http://www.nature.com/ngeo/journal/v9/n4/full/ngeo2670.html?foxtrotcallback=true, 2016.

Su, W., Loeb, N. G., Schuster, G. L., Chin, M., and Rose, F. G.: Global all-sky shortwave direct radiative forcing of anthropogenic aerosols from combined satellite observations and GOCART simulations, Journal of Geophysical Research: Atmospheres, 118, 655–669, doi:10.1029/2012jd018294, https://doi.org/10.1029/2012jd018294, 2013.

Taylor, K. E., Williamson, D., and Zwiers, F.: The sea surface temperature and sea-ice concentration boundary conditions for AMIP II simulations, Program for Climate Model Diagnosis and Intercomparison, Lawrence Livermore National Laboratory, University of California, 2000.

Theil, H.: A rank-invariant method of linear and polynomial regression analysis. I, Nederl. Akad. Wetensch., Proc., 53, 386–392 = Indagationes Math. 12, 85–91 (1950), http://www.ams.org/mathscinet-getitem?mr=0036489, 1950.

Twomey, S.: Pollution and the planetary albedo, Atmos. Environ., 8, 1251–1256, doi:10.1016/0004-6981(74)90004-3, http://www.sciencedirect.com/science/article/pii/0004698174900043, 1974.

van der A, R. J., Mijling, B., Ding, J., Koukouli, M. E., Liu, F., Li, Q., Mao, H., and Theys, N.: Cleaning up the air: effectiveness of air quality policy for SO_2 and NO_x emissions in China, Atmos. Chem. Phys., 17, 1775–1789, doi:10.5194/acp-17-1775-2017, https://www.atmos-chem-phys.net/17/1775/2017/, 2017.

van der Werf, G. R., Randerson, J. T., Giglio, L., van Leeuwen, T. T., Chen, Y., Roĝers, B. M., Mu, M., van Marle, M. J. E., Morton, D. C., Collatz, G. J., Yokelson, R. J., and Ǩasibhatla, P. S.: Global fire emissions estimates during 1997–2016, Earth System Science Data, 9, 697–720, doi:10.5194/essd-9-697-2017, https://www.earth-syst-sci-data.net/9/697/2017/, 2017.

van Marle, M. J. E., Kloster, S., Magi, B. I., Marlon, J. R., Daniau, A.-L., Field, R. D., Arneth, A., Forrest, M., Hantson, S., Kehrwald, N. M., Knorr, W., Lasslop, G., Li, F., Mangeon, S., Yue, C., Kaiser, J. W., and van der Werf, G. R.: Historic global biomass burning emissions for CMIP6 (BB4CMIP) based on merging satellite observations with proxies and fire models (1750–2015), Geosci. Model Dev., 10, 3329–3357, doi:10.5194/gmd-10-3329-2017, https://doi.org/10.5194/gmd-10-3329-2017, 2017.

Wang, S., Xing, J., Jang, C., Zhu, Y., Fu, J. S., and Hao, J.: Impact Assessment of Ammonia Emissions on Inorganic Aerosols in East China Using Response Surface Modeling Technique, Environ. Sci. Technol., 45, 9293–9300, doi:10.1021/es2022347, http://dx.doi.org/10.1021/es2022347, 2011.

Wang, Y., Zhang, Q., Jiang, J., Zhou, W., Wang, B., He, K., Duan, F., Zhang, Q., Philip, S., and Xie, Y.: Enhanced sulfate formation during China's severe winter haze episode in January 2013 missing from current models, J. Geophys. Res. Atmos., 119, 2013JD021 426, doi:10.1002/2013JD021426, http://onlinelibrary.wiley.com/doi/10.1002/2013JD021426/abstract, 2014a.

Wang, Z., Schaaf, C. B., Strahler, A. H., Chopping, M. J., Román, M. O., Shuai, Y., Woodcock, C. E., Hollinger, D. Y., and Fitzjarrald, D. R.: Evaluation of MODIS albedo product (MCD43A) over grassland, agriculture and forest surface types during dormant and snow-covered periods, Remote Sens. Environ., 140, 60–77, doi:10.1016/j.rse.2013.08.025, http://www.sciencedirect.com/science/article/pii/S0034425713002836, 2014b.

Warner, J. X., Dickerson, R. R., Wei, Z., Strow, L. L., Wang, Y., and Liang, Q.: Increased atmospheric ammonia over the world's major agricultural areas detected from space, Geophys. Res. Lett., p. 2016GL072305, doi:10.1002/2016GL072305, http://onlinelibrary.wiley.com/doi/10.1002/2016GL072305/abstract, 2017.

Wielicki, B. A., Barkstrom, B. R., Harrison, E. F., Lee, R. B., Louis Smith, G., and Cooper, J. E.: Clouds and the Earth's Radiant Energy System (CERES): An Earth Observing System Experiment, Bull. Amer. Meteor. Soc., 77, 853–868, doi:10.1175/1520-0477(1996)077<0853:CATERE>2.0.CO;2, http://journals.ametsoc.org/doi/abs/10.1175/1520-0477(1996)077%3C0853%3ACATERE%3E2.0.CO%3B2, 1996.

Wielicki, B. A., Barkstrom, B. R., Baum, B. A., Charlock, T. P., Green, R. N., Kratz, D. P., Lee, R. B., Minnis, P., Smith, G. L., Wong, T., Young, D. F., Cess, R. D., Coakley, J. A., Crommelynck, D. A. H., Donner, L., Kandel, R., King, M. D., Miller, A. J., Ramanathan, V., Randall, D. A., Stowe, L. L., and Welch, R. M.: Clouds and the Earth's Radiant Energy System (CERES): algorithm overview, IEEE Trans. Geosci. Remote Sens., 36, 1127–1141, doi:10.1109/36.701020, 1998.

Wild, M.: Global dimming and brightening: A review, Journal of Geophysical Research: Atmospheres, 114, D00D16, doi:10.1029/2008JD011470, http://onlinelibrary.wiley.com/doi/10.1029/2008JD011470/abstract, 2009.

Xing, J., Mathur, R., Pleim, J., Hogrefe, C., Gan, C.-M., Wong, D. C., and Wei, C.: Can a coupled meteorology–chemistry model reproduce the historical trend in aerosol direct radiative effects over the Northern Hemisphere?, Atmos. Chem. Phys., 15, 9997–10 018, doi:10.5194/acp-15-9997-2015, https://www.atmos-chem-phys.net/15/9997/2015/, 2015.

Yevich, R. and Logan, J.: An assessment of biofuel use and burning of agricultural waste in the developing world., Global Biogeochem. Cycles, 17, 1095, 2003.

Zhang, L., Chen, Y., Zhao, Y., Henze, D. K., Zhu, L., Song, Y., Paulot, F., Liu, X., Pan, Y., and Huang, B.: Agricultural ammonia emissions in China: reconciling bottom-up and top-down estimates, Atmos. Chem. Phys. Discuss., 2017, 1–36, doi:10.5194/acp-2017-749, https://www.atmos-chem-phys-discuss.net/acp-2017-749/, 2017.

Zhang, Q., Streets, D. G., Carmichael, G. R., He, K. B., Huo, H., Kannari, A., Klimont, Z., Park, I. S., Reddy, S., Fu, J. S., Chen, D., Duan, L., Lei, Y., Wang, L. T., and Yao, Z. L.: Asian emissions in 2006 for the NASA INTEX-B mission, Atmos. Chem. Phys., 9, 5131–5153, doi:10.5194/acp-9-5131-2009, https://www.atmos-chem-phys.net/9/5131/2009/, 2009.

Zhao, B., Jiang, J. H., Gu, Y., Diner, D., Worden, J., Liou, K.-N., Su, H., Xing, J., Michael Garay, and Huang, L.: Decadal-scale trends in regional aerosol particle properties and their linkage to emission changes, Environ. Res. Lett., 12, 054 021, doi:10.1088/1748-9326/aa6cb2, http://stacks.iop.org/1748-9326/12/i=5/a=054021, 2017.

Zheng, B., Zhang, Q., Zhang, Y., He, K. B., Wang, K., Zheng, G. J., Duan, F. K., Ma, Y. L., and Kimoto, T.: Heterogeneous chemistry: a mechanism missing in current models to explain secondary inorganic aerosol formation during the January 2013 haze episode in North China, Atmos. Chem. Phys., 15, 2031–2049, doi:10.5194/acp-15-2031-2015, http://www.atmos-chem-phys.net/15/2031/2015/, 2015.

Zhu, Z., Piao, S., Myneni, R. B., Huang, M., Zeng, Z., Canadell, J. G., Ciais, P., Sitch, S., Friedlingstein, P., Arneth, A., Cao, C., Cheng, L., Kato, E., Koven, C., Li, Y., Lian, X., Liu, Y., Liu, R., Mao, J., Pan, Y., Peng, S., Peñuelas, J., Poulter, B., Pugh, T. A. M., Stocker, B. D., Viovy, N., Wang, X., Wang, Y., Xiao, Z., Yang, H., Zaehle, S., and Zeng, N.: Greening of the Earth and its drivers, Nature Climate Change, 6, 791–795, doi:10.1038/nclimate3004, https://doi.org/10.1038/nclimate3004, 2016.